GENESIS AND DISTRIBUTION OF GOLD DEPOSITS IN NYAKISHENYI VILLAGE, BUHWEJU DISTRICT, SOUTHWESTERN UGANDA

NIWAHEREZA PATIENCE

2023/HD13/3054U

BPMM, (NKU)

A DISSERTATION SUBMITTED TO THE DIRECTORATE OF GRADUATE TRAINING IN PARTIAL FULFILMENT OF THE REQUIREMENTS FOR THE AWARD OF MASTER OF SCIENCE DEGREE IN GEOLOGY OF MAKERERE UNIVERSITY

FEBRUARY, 2026

DECLARATION

I **Niwahereza Patience** hereby declare that this dissertation titled "Genesis and distribution of gold deposits in Nyakishenyi village, Buhweju district" is my original work. This report has not been submitted for another degree or qualification at any institution.

Signed ..... Date ...05/02/2026...

Niwahereza Patience

APPROVAL

This dissertation has been submitted for examination with the approval of my university Supervisors listed below:

Signature..... Date 05/02/2026

DR .KEVIN AANYU

DEPARTMENT OF GEOLOGY AND PETROLEUM STUDIES

MAKERERE UNIVERSITY

Signature..... Date 05/02/2026

DR .MUKIIBI SSEWANNYAGA IVAN

DEPARTMENT OF GEOLOGY AND PETROLEUM STUDIES

MAKERERE UNIVERSITY

DEDICATION

This dissertation is dedicated to my husband, Mr. Twinomuhwezi Emmanuel, whose unwavering support and encouragement have been the cornerstone of my academic journey. I also extend heartfelt gratitude to my mother, Mrs. Edith Kyohairwe Baryahikayo, and my children Agaba Ethan Bitindi, Agiira Erol Bitindi, and Ahereza Priyanka Elin whose love and patience have been a constant source of strength.

ACKNOWLEDGEMENTS

I am grateful for the support from Department of Geological Survey for authorization to use their laboratories for analyses and Buhweju district local government authorities for allowing me access the study area and this made possible for me to achieve research target.

Also, my deepest appreciation goes Department of Geology and Petroleum Studies, Makerere University for the providing research materials and academic guidance especially through my supervisors Dr. Kevin and Dr. Mukiibi Ivan for dedicating their precious time in reviewing my work always with constructive scientific ideas and information which this has enabled me to learn a lot of things that have helped me produce quality work and will forever hold you dearly in my heart.

I acknowledge the support of Mr. Muhwezi Deus Katomi, Principal Geochemist from Department of Geological Survey for guidance in understanding and integrating geochemical data and his contribution during discussions with him.

My sincere gratitude also goes to other members of staff from Department of Geological Survey especially Petrology, Assay Lab, Mineral dressing Lab and Cartography. My appreciation goes to lecturers of Master of Geology program at Makerere University for their valuable support at different stages of the project. Thanks go to Masters of Science of Geology students: Mbonye Isaac, Nankinga Stella, Niwagaba Allan, Busingye Ambrose and Nkindo Hillary for their help during laboratory work, discussions and classwork. We have been together during my study in both research and social aspects.

Last but not least, I extend my special thanks to my beloved husband and the entire family for their support, courage and patience during the whole period when I was away from home.

TABLE OF CONTENTS

LIST OF FIGURES

LIST OF TABLES

APPENDICES

LIST OF ACRONYMS

AAS	Atomic Absorption Spectromet
Au	Gold
CF	Concetration Factor
DGS	Department of Geological Survey
DRC	Democratic Republic of Congo
GIS	Geographic Information System
GPS	Global Positioning System
GTK	Geological Survey of Finland (from context of GTK Consortium)
ICP-MS	Inductively Coupled Plasma Mass Spectrometry
IDW	Inverse Distance Weighting
MEMD	Ministry of Energy and Mineral Development
QA/QC	Quality Assuarance/Quality Control
RIRGD	Reduced Intrusion-Related Gold Deposits
SDGs	Sustainable Development Goals
SMRP	Sustainable Management of Mineral Resources Project
UN	United Nations

ABSTRACT

This study investigates the genesis and spatial distribution of gold deposits in Nyakishenyi Village, Buhweju District, South Western Uganda, with the main aim of understanding the structural and geochemical controls of orogenic gold systems. The study area is found within the Proterozoic Kibaran Belt and this region represents a geologically significant yet underexplored segment of Uganda's Precambrian terranes.

Quartz veins within schists, quartzites, and granitoid contacts host the primary gold deposits, with NW–SE and NE–SW trending shear zones and faults acting as key fluid pathways.Primary gold mineralization is concentrated at lithological boundaries and fault – fault intersections, reinforced by elevated pathfinder elements (e.g As, Sb, Cu, W) confirming an orogenic origin. Secondary placer deposits in colluvial zones and stream channels represent erosional derivatives of the primary lodes.

GIS modeling exposed strong links between fault density, structural intersections, geochemical anomalies, and artisanal mining spots. Quartz veins reverted peak gold grades of 1.65 ounces per ton. averaging 0.5–1.2 ounces per ton. in shear zones, while placer deposits generated 0.3–0.8 g/t, indicating secondary enrichment. High-grade zones averaged 2.5 faults/km², with mineralization hotspots concentrated at fault intersections and lithological contacts between schists, quartzites, and granitoids.

Elevated pathfinder elements (As, Sb, Cu, W) frequently align with high gold values (>1.5 oz/t), while major oxides (Fe_2O_3, Al_2O_3, Na_2O) specify hydrothermal alteration, confirming the orogenic nature of the gold system. Nyakishenyi hosts both structurally controlled orogenic gold deposits and secondary placer accumulations. Integrating structural and geochemical data provides a strong predictive framework for future exploration in the Kibaran Belt and similar Precambrian terrains.

CHAPTER ONE
INTRODUCTION

1.1 Background

Gold is a globally significant mineral with economic, industrial, and cultural value. Its unique physical and chemical properties, combined with sustained global demand, make it a key target for mineral exploration (Groves et al., 1998). In Africa, major gold deposits occur in Archaean and Proterozoic greenstone belts, with structurally controlled orogenic systems dominating production in countries such as Ghana, South Africa, and Mali (Grynberg et al., 2021). In East Africa, greenstone belts and rift-related structures, particularly in Tanzania and Kenya, host shear-zone-controlled and stratiform gold deposits (Kuehn et al., 1990).

Uganda's Proterozoic basement complex contains several gold districts, including Busia, Mubende, Karamoja, and Buhweju (figure 1.1). While Busia and Karamoja have been studied extensively, Buhweju remains underexplored despite active artisanal mining (Abraham et al., 2020; Bahiru, 2011). The district lies within the mesoproterozoic Kibaran Belt, characterized by deformed metasedimentary rocks-quartzites, schists, and phyllites—hosting structurally controlled quartz-carbonate veins (Tack et al., 2010). Artisanal and small-scale gold mining in valleys and river channels reflects secondary placer deposits derived from primary lode sources, but the origins, spatial distribution, and controls on gold mineralization remain poorly documented (van der Ven, 2020; Serwajja & Mukwaya, 2021).

Previous studies highlight the presence of gold-bearing quartz veins, but there is limited information on whether these deposits are orogenic, hydrothermal, or otherwise, and primary versus secondary occurrences are not well mapped. The lack of systematic geological mapping, structural analysis, and geochemical surveys has constrained exploration, resource evaluation, and informed policy development.

This study addresses these gaps by applying integrated geological, structural, and geochemical methods to assess the genesis and spatial distribution of gold deposits in Nyakishenyi village, Buhweju District. Field mapping, petrography, and geochemical analyses (ICP-MS and XRF) combined with GIS-based spatial modeling provide a robust framework for understanding mineralization processes, guiding exploration, and supporting sustainable resource management in the district. The outcomes will also contribute to regional metallogenic knowledge and inform responsible mining strategies aligned with national development goals.

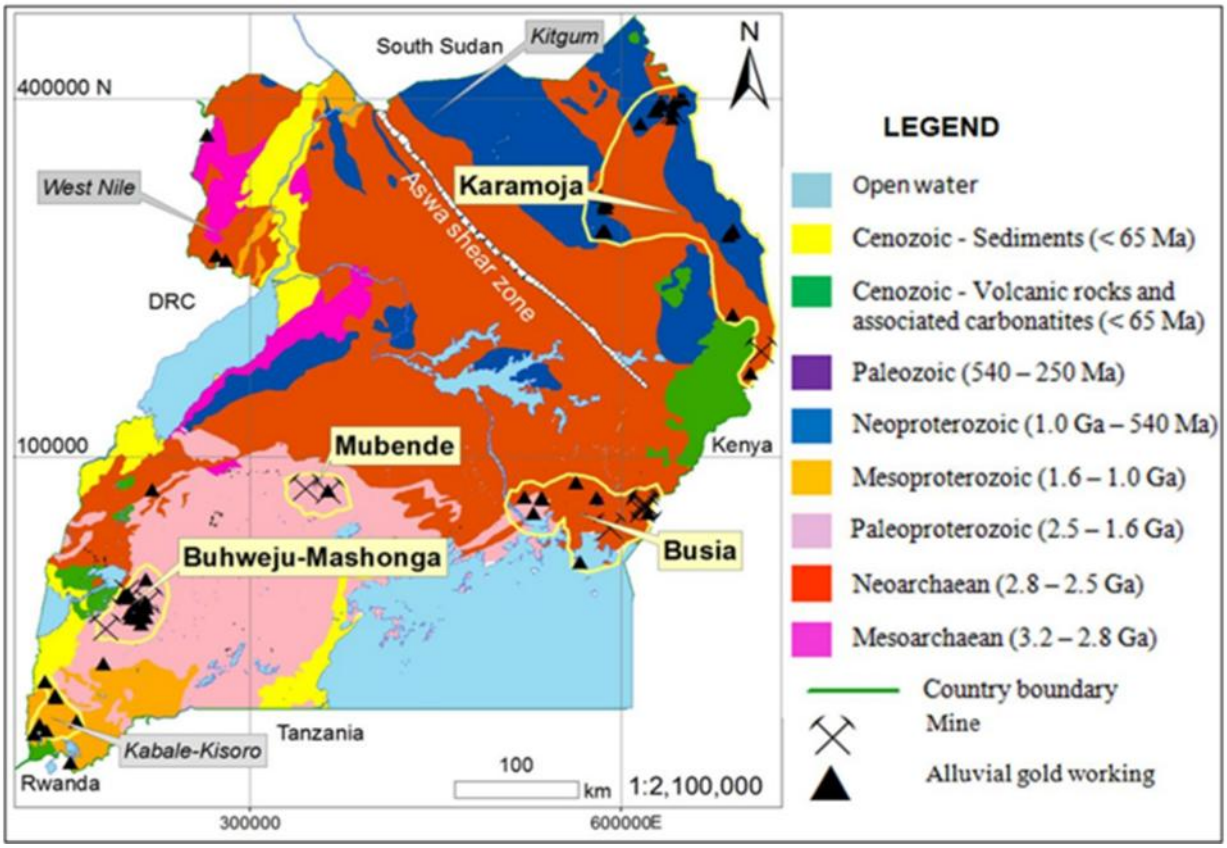

Figure 1.1*: Map showing the location of the major gold districts in Uganda: Buhweju – Mashonga, Mubende, Karamoja and Busia. (Source DGS).*

1.1.1 Regional and local geological setting of Buhweju District

Uganda lies within the tectonically active East African Rift System and hosts a geologically diverse landscape enriched with mineral resources, particularly gold. The country's deposits are predominantly orogenic, formed during compressional deformation in accretionary orogens, with hydrothermal fluids concentrating mineralization within greenstone belts. These deposits, hosted in Archean and Paleoproterozoic terrains, share genetic similarities with globally recognized provinces such as the Yilgarn Craton in Australia and the Birimian Supergroup of West Africa (Groves & Bierlein, 2007). Within Uganda, significant occurrences have been documented in Busia, Karamoja, and Buhweju districts (Gabert, 1990), though systematic exploration remains limited.

Buhweju District, located in southwestern Uganda's mineral-rich western corridor, lies within the Kibaran Supergroup—a Mesoproterozoic orogenic belt extending into Rwanda, Burundi, and the eastern DRC. The belt records major tectonic events, including the Bukoba Orogeny (~1.3 Ga), which folded and metamorphosed metasedimentary sequences, and syn-tectonic granite emplacement (~1.2–1.0 Ga), which enhanced metamorphism and hydrothermal activity, contributing to gold-bearing quartz-carbonate vein formation (Tack et al., 2010). Later reactivation linked to the East African Rift System further modified structural fabrics, enhancing permeability along shear zones and faults. Buhweju is underlain by deformed quartzites, phyllites, and schists, with multiple deformation phases producing shear zones, fold hinges, and fault systems that act as conduits for mineralizing fluids.

Gold mineralization in Buhweju is primarily hosted in narrow quartz-carbonate veinlets within schist formations, often associated with sulfide minerals such as galena, chalcopyrite, and pyrite (Nuwagira et al., 2023). Historical studies described sulfide-bearing quartz reefs (Barnes et al., 1961) and a significant ore body within a dolerite dyke striking N20°E and dipping 45° SE, with sheared contacts against quartz-biotite gneiss (Cratchley & Evans, 1967), highlighting strong structural controls. Secondary occurrences in alluvial and colluvial environments, particularly valley bottoms and stream channels, sustain artisanal and small-

scale gold mining (ASGM), though activities remain informal and poorly documented (Abraham et al., 2020). Despite its mineral potential, Buhweju remains underexplored, with limited geological mapping and geochemical surveys. Establishing a scientific framework for gold genesis and distribution in Nyakishenyi Village is therefore critical to guiding exploration, reducing resource wastage, and supporting Uganda's broader goals for responsible mining and sustainable resource management (Serwajja & Mukwaya, 2021).

1.1. Problem statement

Buhweju District in southwestern Uganda hosts numerous gold occurrences and supports significant artisanal gold mining that contributes to local livelihoods and national development. The district is underlain by Proterozoic metamorphic rocks, shear zones, and fault systems that are favorable for orogenic gold mineralization. However, despite these geological advantages, Buhweju remains one of the least geologically documented gold-bearing districts in Uganda.

The genesis and spatial distribution of gold mineralization in Buhweju are poorly understood due to limited systematic geoscientific investigations. Previous studies have inadequately addressed the structural controls, petrographic characteristics, alteration patterns, and geochemical signatures associated with gold mineralization. In particular, there is a lack of integrated geological mapping, petrographic analysis, and geochemical profiling, as well as insufficient data on pathfinder elements and their spatial relationships to gold occurrences.

As a result of these knowledge gaps, current gold mining in Buhweju is dominated by artisanal and small-scale miners who rely mainly on surface indications and historical information rather than scientific exploration data. This has led to ineffective targeting of mineralized zones, low gold recovery rates, unsafe mining practices, and environmentally unsustainable operations. The absence of a scientific framework for understanding gold mineralization also limits informed exploration planning and resource management in the district.

1.3. Objectives

1.3.1. Major objective

The main objective was to assess the genesis and distribution of gold deposits in Nyakishenyi village, Buhweju district.

1.3.2. Specific objectives

The specific objectives for this study included:

i. To determines geochemical gold composition in primary and secondary ores occurrences.
ii. To characterize gold deposits in Buhweju
iii. To map spatial distribution of geological features in the area

1.4. Significance of the study

This research contributes directly to Sustainable Development Goal (SDG) 12, which emphasizes responsible consumption and production. By promoting scientific methods that minimize environmental degradation while enhancing mineral exploitation efficiency, the study supports the development of policies aimed at sustainable economic growth and ethical resource use in the gold supply chain (Monteiro et al., 2019) . It emboldens extraction practices that avoid resource depletion and mitigate ecological harm, aligning with global sustainability frameworks.

The generation of detailed geological and geochemical data on gold deposits in Buhweju District will foster the formalization of artisanal and small-scale mining (ASGM) activities. This aligns with Uganda's National Development Plan IV (2024/25), which prioritizes mineral development as a driver of economic transformation. By providing a scientific basis for exploration, the study will permit government agencies, investors, and mining companies to plan for large-scale mining operations, thereby reducing exploration risks and optimizing investment decisions.

The study also supports Uganda's commitments under the International Conference on the Great Lakes Region (ICGLR) 2011 framework, which promotes responsible mining practices

among member states. By enhancing Uganda's mineral inventory and contributing to traceability and international reporting standards, the research strengthens the country's ability to attract foreign investment and comply with global transparency protocols.

Through the identification of structurally controlled gold deposits and associated pathfinder elements (e.g., As, Sb, Cu, Pb), the study will progress exploration success rates and gold recovery efficiency. This has direct socio-economic significances, including job creation, improved local livelihoods and stimulation of industrial growth in Buhweju District

Ultimately, the findings will serve as a scientific orientation for future mineral exploration initiatives in Uganda and across East Africa, supporting sustainable resource management, policy formulation, and regional economic development.

1.5. Justification of the study

Buhweju District, located within Uganda's mineral-rich western corridor, remains geologically underexplored and structurally misunderstood despite its recognized potential for gold deposits. Mining activities in the region are largely assumed by artisanal and small-scale miners (ASGM), who rely on informal indicators and surface expressions rather than scientific data. This lack of geoscientific guidance has resulted in inefficient resource recovery, environmental degradation, and heightened occupational risks.

Although previous investigations have established the presence of gold within Buhweju, they have not adequately addressed the petrographic, structural, and geochemical controls governing the genesis and spatial distribution of these deposits. The absence of geochemical maps and pathfinder element datasets such as arsenic (As), antimony (Sb), copper (Cu), and lead (Pb) has constrained systematic exploration. Subsequently, mineralized zones remain poorly delineated, and mining activities continue in geologically unstable or environmentally sensitive areas.

This study adopts a multidisciplinary and precision-driven style to address these challenges. High-resolution geochemical techniques, including Inductively Coupled Plasma Mass Spectrometry (ICP-MS) and Atomic Absorption Spectrometry (AAS), are employed to quantify trace and pathfinder elements with accuracy. These methods facilitate the detection

of subtle geochemical anomalies that are often overlooked by conventional surface-based techniques.

Petrographic analysis using thin sections provides comprehension into mineral assemblages, alteration textures, and paragenetic sequences, facilitating the distinction between barren and mineralized vein systems. Comprehensive field mapping of lithological units, shear zones, and fault orientations supports structural interpretation and the identification of hydrothermal fluid pathways critical for targeting orogenic gold systems.

Geospatial modeling using Geographic Information Systems (GIS) assimilates geochemical anomalies, structural intersections, and ASGM activity to visualize predictive zones of mineralization. This methodology transforms raw field and laboratory data sets into actionable exploration targets. Unlike previous studies, this research does not treat datasets in isolation but links geochemistry, structural geology and petrology to develop a robust mineral targeting framework.

1.6. Scope

This study focuses on Nyakishenyi Village in Buhweju District, a region with a long-standing history of artisanal and small-scale gold mining (ASGM).

A total of 50 geological samples including soils and rocks were systematically collected across a 3 km² area using a high-resolution grid (50 m × 50 m). Soil samples were taken from the B-horizon (0–30 cm depth), while rock samples were sourced from quartz veins, shear zones, and altered outcrops, with emphasis on areas exhibiting pyrite and arsenopyrite mineralization.

Laboratory analyses were conducted at the Directorate of Geological Survey and Mines (DGS) using XRF for major oxides, ICP-MS and AAS for gold and trace elements (As, Cu, Pb, Zn, Sb). Petrographic studies were performed to characterize mineral assemblages, alteration textures, and host rock relationships.

All analytical and spatial data were incorporated using GIS software to generate geochemical anomaly maps. Quality assurance protocols comprising field duplicates, analytical blanks, and certified reference standards were implemented to guarantee data reliability.

The study's integrated methodology combining geological mapping, geochemistry, petrography, and spatial modeling provide a robust framework for understanding the structural and geochemical controls on gold mineralization in Buhweju. It offers a scientific foundation for future exploration and resource development in the region.

1.7. Conceptual model

The conceptual model (figure 1.2) highlights how geological and geochemical factors interact to control the formation and distribution of gold deposits. It shows that the type of gold occurrence (primary or secondary) governs key processes such as hydrothermal fluid evolution, migration, and deposition, which in turn determine geochemical signatures and elemental anomalies. Host rock characteristics, structural controls, alteration, weathering, and petrographic features further modify deposit characteristics. By linking deep-seated geological processes with surface expressions, the model provides an integrated framework for interpreting geochemical data and guiding gold exploration.

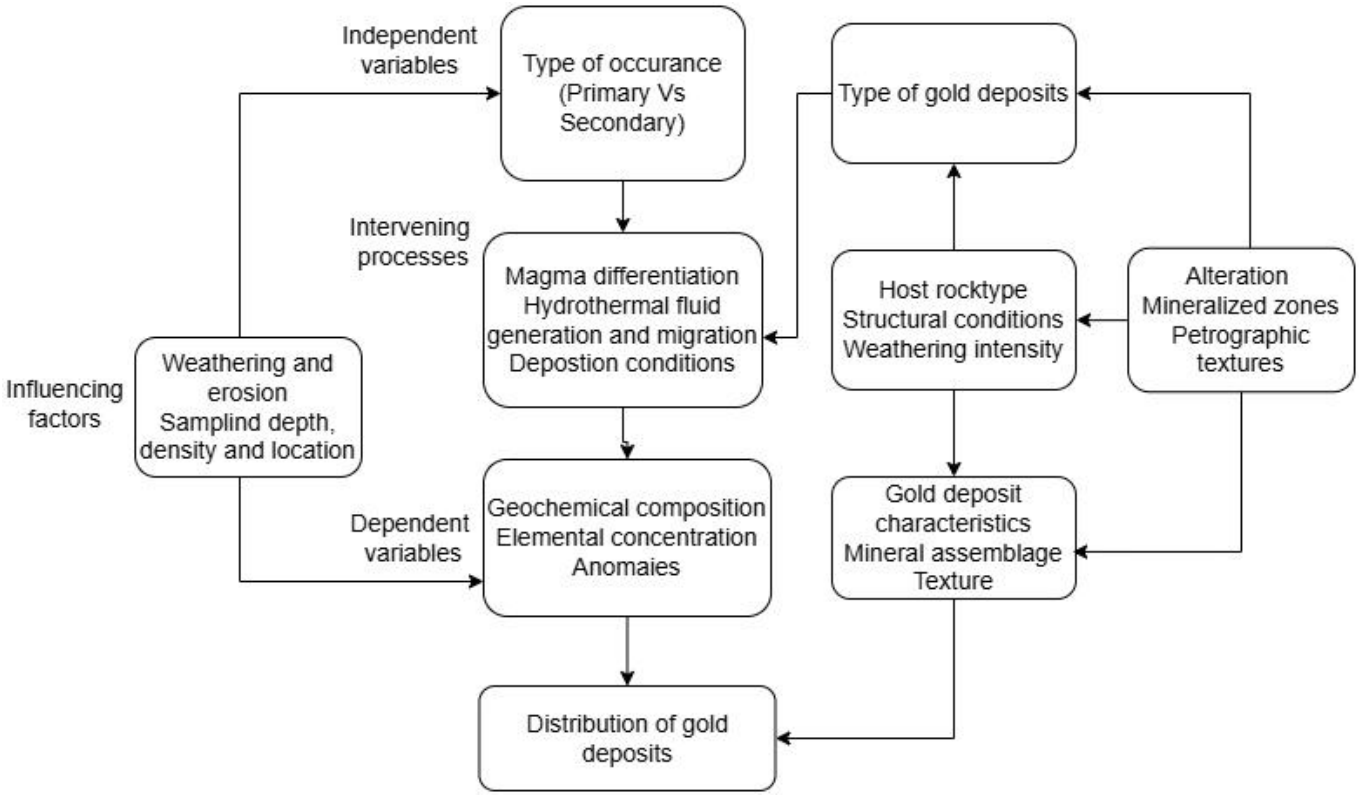

Figure 1.2: *Conceptual model for genesis and distribution of gold deposits in Nyakishenyi village, Buhweju district.*

CHAPTER TWO
LITERATURE REVIEW

2.1 Global Gold Deposits: Types and models of Gold deposits occur in diverse geological settings and are classified according to their formation processes, host lithologies, mineral assemblages, and structural controls. Understanding these deposit types provides a conceptual framework that guides exploration strategies and informs the methodology of this study. Globally, five principal models are recognized: orogenic gold systems, placer deposits, epithermal systems, intrusion-related deposits, and Carlin-type deposits (figure 2.1). While all models contribute to comparative understanding, orogenic and placer deposits are most relevant to Buhweju District due to its tectonic architecture and geomorphological conditions.

Orogenic Gold Deposits

Orogenic (mesothermal) gold deposits form during compressional tectonic events associated with crustal thickening, regional metamorphism, and accretionary orogens. These deposits typically develop at mid-crustal depths (5–15 km), under moderate to high temperatures (250–450°C) and pressures (1–5 kbar). Mineralizing fluids are CO_2–H_2O-rich, low-salinity hydrothermal solutions derived from metamorphic devolatilization. As these fluids migrate through brittle-ductile structures such as shear zones, faults, and fold hinges, gold precipitates in quartz-carbonate veins due to changes in pressure, temperature, or chemical environment (Groves et al., 1998; Goldfarb et al., 2005).

The Kibaran Belt, which hosts Buhweju District, differs tectonically from other Proterozoic mobile belts by recording the Bukoba Orogeny (~1.3 Ga) and subsequent syn-tectonic granite emplacement (~1.2–1.0 Ga). These events produced intense deformation, metamorphism, and hydrothermal activity, creating structurally favorable conduits for mineralizing fluids. Unlike younger Pan-African belts, the Kibaran is characterized by Mesoproterozoic metasedimentary sequences (quartzites, schists, phyllites) that underwent multiple deformation phases, enhancing permeability along shear zones. This tectonic complexity provides a robust orogenic framework for gold mineralization in Buhweju, where sulfide-bearing quartz veins

(pyrite, arsenopyrite, chalcopyrite) are structurally controlled within schists and gneisses.Placer deposits represent secondary accumulations formed by the mechanical concentration of gold particles eroded from primary sources. Gold's high density (19.3 g/cm³) and chemical inertness allow it to resist oxidation and concentrate in low-energy depositional environments such as stream beds, floodplains, and colluvial sediments. Globally, placer systems such as the Witwatersrand Basin (South Africa) and Klondike (Canada) demonstrate the economic significance of fluvial reworking. In Buhweju, rugged topography, tropical weathering, and dense drainage networks facilitate erosion of primary quartz veins and transport of gold particles downslope into valleys and stream channels. These deposits sustain artisanal and small-scale mining (ASGM), though recovery remains inefficient due to lack of scientific guidance.Other Deposit Models

Epithermal, intrusion-related, and Carlin-type deposits provide comparative insights but are less applicable to Buhweju. Epithermal systems require active volcanism, absent in the district. Intrusion-related deposits are linked to felsic magmatism, but Buhweju hosts only minor granitic intrusions with limited mineralization. Carlin-type deposits, characterized by disseminated gold in siliceous sedimentary rocks, are geologically absent due to the lack of suitable host lithologies. The integration of global deposit models into this study provides a predictive framework for exploration in Buhweju. The orogenic model explains the genesis of structurally controlled vein-hosted deposits, guiding structural mapping, petrographic analysis, and geochemical surveys to delineate mineralized zones. The placer model clarifies source-to-sink relationships, informing stream sediment sampling, soil geochemistry, and GIS-based anomaly mapping. By situating Buhweju within the Kibaran Belt's tectonic timeline and contrasting it with other Proterozoic belts, the study establishes a genetic basis for gold mineralization. This conceptual framework directly shapes the methodology, ensuring that field investigations, geochemical analysis, and spatial modeling are aligned with the geological processes most relevant to the district.

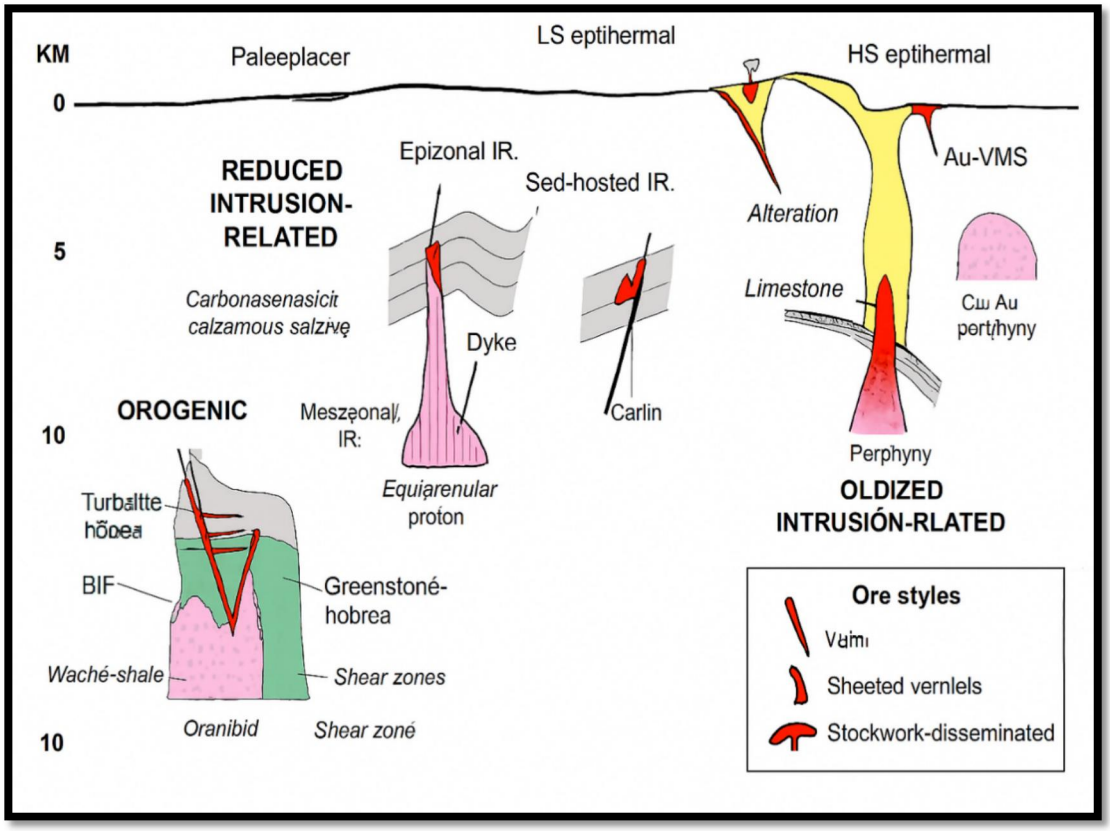

***Figure 2.1**: Schematic cross section showing the key geologic elements of the main gold systems and their crustal depths of emplacement. Note the logarithmic depth scale. Modified from Poulsen et al. (2000), and Robert (2004a).*

2.3. Review of methods and selected approach

Gold distribution and genetic studies necessitate a multidisciplinary approach that integrates geological, petrographic, geochemical, and spatial datasets. Geological mapping and structural analysis are deliberated the most fundamental for documenting lithologies, shear zones, and faults which act as conduits and traps for mineralizing fluids (Groves et al., 1998). Petrographic analysis complements by enlightening mineral assemblages, alteration styles, and deformation textures, though it has always been limited by its point-scale nature (Passchier & Trouw, 2005).

Geochemical methods such as ICP‑MS and fire assay offer quantitative measures of gold and pathfinder elements (Govett, 1983; Levinson, 1980) which bid sensitivity to primary lode signatures and secondary placer dispersion (Rose et al., 1979). These techniques, however, demand strict QA/QC and are vulnerable to contamination (Harris, 1999). Remote sensing and GIS analysis incorporate geological and geochemical data into extrapolative models which produce prospectivity maps (Carranza, 2009; Bonham‑Carter, 1994). Geophysical methods usually add subsurface constraints but often impractical for further studies (Dentith & Mudge, 2014).

This study assumes a combined approach of mapping, petrography, geochemistry, and GIS. The datasets from Nyakishenyi provide straight evidence of gold distribution and pathfinder correlations that have enabled anomaly detection and spatial modeling. GIS integration highpoints zones where structures, reactive lithologies, and anomalies overlap. The approach is comprehensible with orogenic–placer models, and this show indication across datasets, and remains reproducible. Limitations such as sampling representativeness and detection thresholds were moderated through stratified sampling and QA/QC.

Expected outputs include anomaly maps, correlation matrices involving gold with arsenic and antimony, petrographic evidence of alteration, and GIS‑based hotspot maps. These results address the study's purposes such as determining gold composition, characterizing deposit styles, and analyzing spatial distribution, thereby inaugurating a robust framework for exploration in Buhweju.

2.4 Introduction to geological framework

Buhweju District in Western Uganda lies within the East African Orogenic Belt, a zone marked by Precambrian deformation, metamorphism, and mineralization (Thomas et al., 2016). The district comprises high-grade metamorphic rocks and Mesoproterozoic metasedimentary sequences, structurally reworked during the Kibaran (~1375 Ma) and Pan-African (~600 Ma) orogenies (Tack et al., 2010). These tectonic events shaped the

lithological and structural architecture that controls the distribution of orogenic and placer gold deposits.

Structural features shear zones, faults, and folds serve as conduits and traps for hydrothermal fluids, while quartzites, schists, and amphibolites (figure 2.2) provide chemically reactive and mechanically competent hosts (Ambrose, 2019). The interplay of lithology and structure governs gold grade, style, and spatial distribution.

This chapter presents regional geological context of Western Uganda relevant to Buhweju bedrock geology, structural framework, and lithologies affecting gold deposition; The spatial distribution and genesis of gold deposits and review of prior studies to identify exploration gaps (Herbert et al., 2014; Githenya, 2020).

2.4.1 Geological framework of Western Uganda

Western Uganda is underlain by Precambrian basement rocks recording multiple tectonic events. Key units include the Kibaran Belt, Rwenzori Fold Belt, and Toro–Buhweju Terrane, collectively part of the East African Orogenic Belt, a zone of intense deformation, metamorphism, and mineralization (Thomas et al., 2016). Active tectonism and structural reactivation continue to enhance hydrothermal fluid pathways, favoring mineral deposition (Reece, 1961).

The basement consists of Archaean–Paleoproterozoic high-grade gneisses, granulites, amphibolites, and migmatites, forming a crystalline foundation for overlying metasedimentary sequences (Schlüter, 2008). The Mesoproterozoic Kibaran Belt, trending NW–SE, comprises quartzites, phyllites, pelitic schists, and metaconglomerates, which are primary hosts for orogenic gold. Tectonism, metamorphism, and granitic intrusions during the Kibaran Orogeny (~1375 Ma) created structural traps and fluid conduits conducive to mineralization (Tack et al., 2010).

The Rwenzori Fold Belt is characterized by highly deformed basement blocks, faults, folds, and granitoid intrusions, which enhance permeability and fluid flow. Granitic and granodioritic intrusions, often syn-tectonic, generated thermal and structural conditions

favorable for hydrothermal remobilization, vein formation, and localized gold deposition (Pohl, 1994).

Lithologically, quartzites and schists dominate Buhweju, forming the main host rocks for structurally controlled orogenic gold, while amphibolites and gneisses intercalated within these sequences host sulfides and act as fluid traps (Ambrose, 2019).

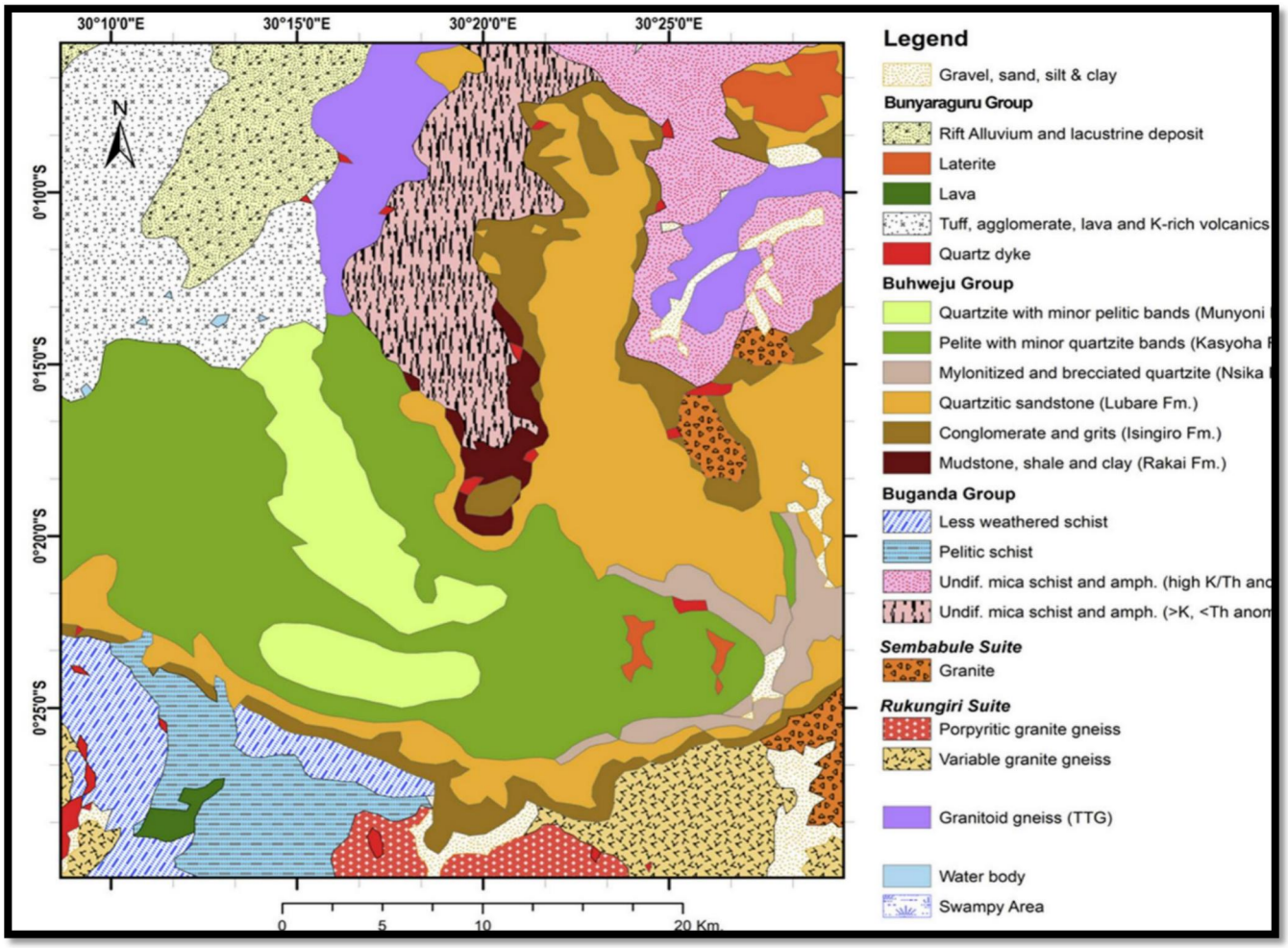

Figure 2.2: *Geological map of Buhweju area (modified after Bahiru (2011); Lehto et al. (2014a); Bahiru and Woldai (2016).*

2.4.2. Structural geology of Buhweju district.

Buhweju District in southwestern Uganda is structurally complex, having undergone multiple phases of deformation, faulting, and metamorphism that strongly influence gold mineralization. The district is characterized by folded and faulted terrains, with major shear zones trending NNE–SSW and NW–SE. These structures act as conduits for hydrothermal fluids, enabling gold precipitation along zones of enhanced permeability (Admassu, 2011).

Isoclinal folds are common in schists and phyllites, reflecting ductile deformation and providing traps for mineralizing fluids. Fractures and minor faults enhance permeability in competent lithologies such as quartzites and gneisses, which serve as favorable hosts for structurally controlled mineralization (Admassu, 2011).

Metamorphism in Buhweju ranges from greenschist to amphibolite facies, typical of orogenic gold systems. Retrograde textures and recrystallized quartz veins confirm a dynamic, multi-phase deformation history, consistent with regional tectonic evolution (Priscillah, 2022).

Hydrothermal alteration is prominent around auriferous veins, including silicification (quartz enrichment), sericitization (fine-grained mica alteration), ferruginization (iron oxide staining linked to sulfide breakdown), and chloritization (chlorite development in mafic units). These alteration assemblages are reliable indicators of fluid pathways and mineralization zones (Sherlock, 2016).

Buhweju hosts both primary and secondary gold deposits. Primary mineralization occurs in quartz veins within schists, phyllites, and quartzites, localized along shear zones and fracture networks. Secondary deposits are concentrated in lateritic soils, colluvial sediments, and stream beds, forming placer systems actively exploited by artisanal miners (Backman et al., 2014). Despite widespread artisanal activity, Buhweju remains underexplored, with limited formal geological mapping and geochemical evaluation. This presents significant opportunities for integrated structural mapping, petrographic analysis, and geochemical targeting to delineate new mineral prospects. The district's structural complexity, metamorphic framework, and alteration signatures provide a strong basis for applying

orogenic and placer deposit models to guide exploration strategies (Admassu, 2011; Schumann et al., 2015).

2.5. Genesis of gold deposits in Buhweju

The genesis of gold deposits in Buhweju district is primarily linked to orogenic processes associated with the Proterozoic Kibaran belt, a structurally controlled and metamorphosed terrane in Western Uganda (Bahiru & Woldai, 2016). These deposits are the outcome of a multi-phase geological history involving tectonic deformation, regional metamorphism, hydrothermal fluid activity, and surface weathering (Bahiru, 2011) .

The district is underlain by Mesoproterozoic metasedimentary rocks of the Kibaran Super group, composed predominantly of quartzites, micaceous and pelitic schists, phyllites, and minor amphibolites and granitoids. These lithologies have undergone intense folding, shearing, and faulting, creating them favorable hosts for structurally controlled gold mineralization. Dominant structural features include shear zones, foliation planes, fold hinges, joints, fracture networks, and fault zones, which act as fluid conduits and traps for mineralizing solutions (Reece, 1961) .

Globally, gold deposits are classified into numerous genetic types, including orogenic (mesothermal), epithermal, porphyry, skarn, and placer systems. Among these, orogenic gold deposits are the most appropriate to Buhweju's geological context. These deposits typically form during regional metamorphism and compressional tectonics, where low-salinity, CO_2-rich metamorphic fluids migrate along crustal structures and precipitate gold in quartz veins due to changes in pressure, temperature, and fluid-rock interaction (Sillitoe, 2020) .

The Kibaran belt, which spans parts of Uganda, Rwanda, Burundi, and the Democratic Republic of Congo, is a Mesoproterozoic mobile belt known for its structurally controlled mineralization. It was formed through continent–continent collision and crustal thickening, creating favorable conditions for hydrothermal fluid circulation and orogenic gold formation (Tack et al., 2010). Analogous deposits in the Twangiza–Namoya gold belt of eastern DRC display related geological settings, where gold is hosted in shear-zone quartz veins within

metasedimentary rocks, reinforcing the genetic model applicable to Buhweju (Kampunzu et al., 2009).

Further studies approve that Buhweju's gold deposits occur in both primary and secondary environments. Primary mineralization is associated with deformed quartzites and micaceous schists, where NW–SE and NE–SW trending shear zones serve as conduits for hydrothermal fluids. Gold precipitation is compelled by fluid-rock interactions, pressure drops, and temperature gradients within these shear structures (Robert et al., 1997).

Previous regional and site-specific surveys support this genetic interpretation, reinforcing the scientific basis for ongoing exploration. The integration of structural mapping, lithological analysis, and fluid inclusion studies continues to augment understanding of Buhweju's mineral systems and guide future resource development.

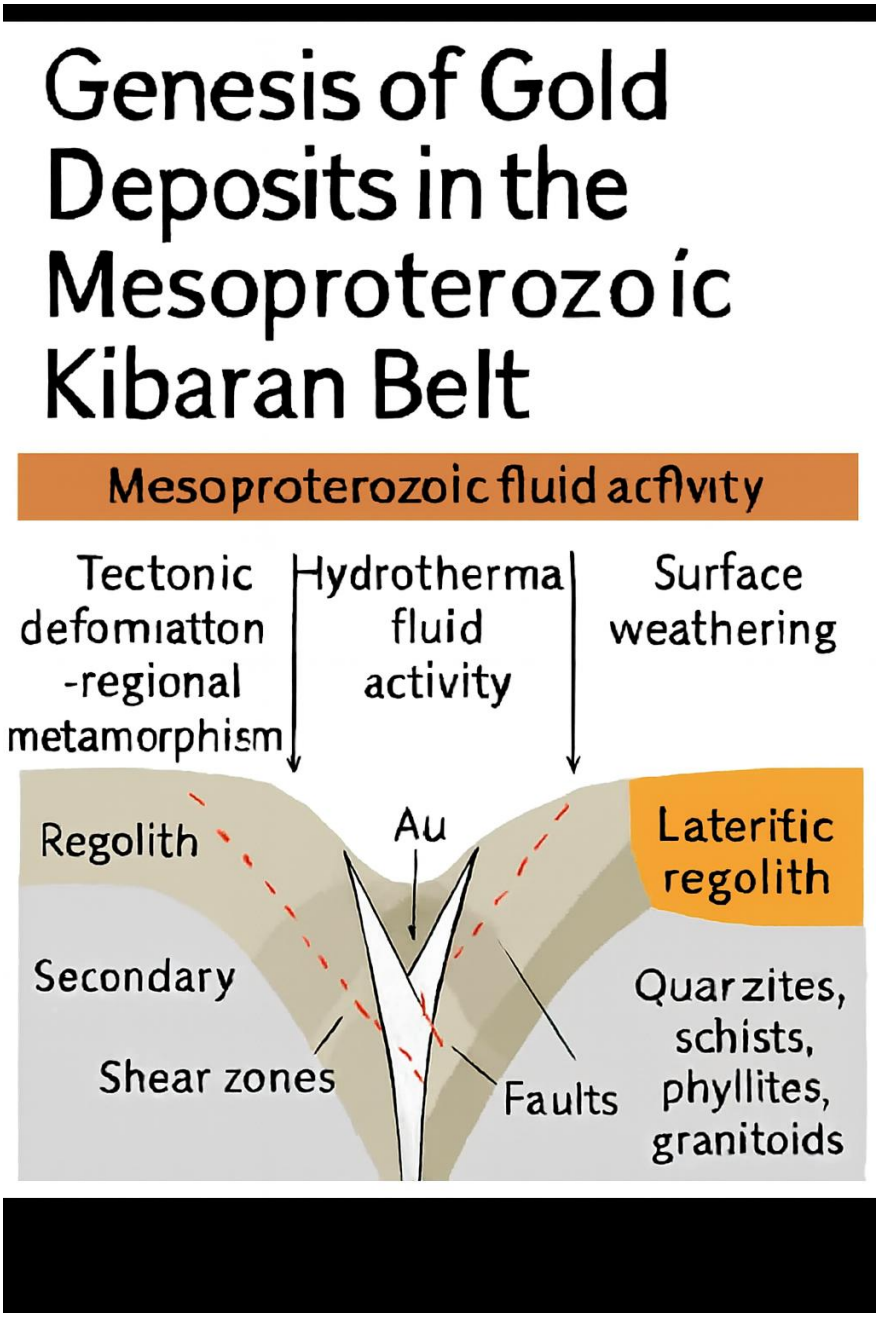

Figure 2.3: *Conceptual illustration showing the genesis of gold deposits in the Mesoproterozoic Kibaran Belt. The diagram highlights key geological processes including tectonic deformation, regional metamorphism, hydrothermal fluid activity, and surface weathering. Gold deposits are structurally controlled, occurring in quartz veins within shear zones and faults, and also concentrated in lateritic regolith through secondary enrichment. Source (Reece, 1998).*

2.6. Spatial distribution of gold deposits in Buhweju

Gold deposits in Uganda are disseminated across several districts, including Buhweju, Mubende, Busia, Karamoja, and Namayingo, with Buhweju recognized as one of the most active artisanal mining regions. The spatial distribution of gold in Buhweju is intensely influenced by structural controls, lithological variations, and geomorphological settings, with deposits occurring in both primary quartz veins and secondary regolith-hosted environments.

Located in the southwestern part of Buhweju District, Kyankanda is the most prominent artisanal mining site. Gold is principally recovered from weathered schists, and geochemical analysis exposes elevated concentrations of Au up to 3.5 ppm, indicating significant enrichment in the oxidized zone (Backman et al., 2014) . The site is structurally aligned with NW–SE trending shear zones, which act as conduits for mineralizing fluids.

The Kashenyi area hosts quartz vein systems within micaceous schists and phyllites, with gold recuperated from lateritic soils and narrow vein zones during artisanal operations. Soil geochemical surveys report gold values ranging from 0.5 to 2.7 ppm, with enrichment zones spatially correlated with structural lineaments, signifying a strong structural control on mineralization.

In Nyarwambu, mining activities focus on lateritic soils that exhibit high surface enrichment. Gold concentrations reach up to 1.8 ppm, and field mapping has identified NW-trending shear zones, which are interpreted as the primary structural features guiding fluid flow and ore localization.

Situated near the central Buhweju ridge, Karungu shows both primary and secondary gold occurrences. Quartz veins cross-cut foliated metasedimentary rocks, and stream sediment geochemical analysis discloses anomalous gold values exceeding 100 ppb, with associated enrichment in Fe, Mn, and As. These multi-element anomalies recommend hydrothermal alteration and possible sulfide association.

The Burambira mining site shows indication of historical mining, with scattered quartz float interpreted as remnants of eroded veins. Soil samples from the area report gold concentrations ranging between 0.3 and 1.6 ppm Au, indicating residual enrichment in the

weathered zone (Staudt et al., 2014). The spatial distribution of gold in Buhweju reflects a amalgamation of: lithological favorability (quartzites, schists, phyllites), structural permeability (shear zones, faults, joints) and geomorphological concentration (lateritic soils, stream sediments). This pattern emphasizes the need for integrated structural mapping, geochemical profiling, and remote sensing analysis to delineate prospective zones for future exploration.

2.7. Previous studies on gold deposits in Buhweju

The Buhweju district is recognized as one of Uganda's primary gold- and base-metal-producing regions. Despite its long-standing artisanal mining activity, detailed scientific understanding of the genesis, distribution, and structural controls of gold deposits remains limited. Most gold occurrences in Buhweju appear to be genetically linked to post-Kibaran orogenic events, with two main mineralization episodes identified: one associated with post-orogenic rifting, and another related to post-orogenic metamorphism (Pohl, 2011).

Within the Buhweju Group, various lithological units exhibit bedding planes, cleavages, and linear structures, which have been interpreted as evidence of WNW-trending folding, with deformation intensity increasing toward the southern part of the district (Bahiru, 2011). These structural features are considered critical in controlling the localization of gold-bearing veins and alteration zones.

According to Reece (1961), field observations and thin-section petrography indicate that Buhweju has undergone significant tectonic thickening. Structural features such as foliations and lineations are common in schists, quartzites, and gneisses of the Igara Group. Gneissic rocks display a nearly parallel NW-trending foliation, marked by mineral banding and a preferred orientation of feldspar porphyroblasts. In schists, foliation is defined by aligned white mica flakes, forming weak planes. The primary foliation corresponds to early NNW-trending isoclinal folds, while a secondary foliation, described as slip cleavage, is evidenced by drag folds and fracture cleavage, superimposed on earlier deformation phases.

The Department of Geological Survey and Mines (DGSM) documented gold occurrences in Kashenyi, Karungu, and Kyankanda, noting their alignment with regional foliation and shear

zones. Geochemical analyses from these sites revealed elevated concentrations of Au, As, and Fe, consistent with an orogenic gold system (Chen et al., 2006) . These findings support the interpretation that gold deposits in Buhweju are structurally controlled and genetically linked to metamorphic-hydrothermal processes.

Gold deposits in Buhweju are predominantly alluvial, occurring in lateritic soils and stream sediments, although reef-type gold associated with sulfide-bearing quartz veins has also been documented (Wayland, 1934). Informal mining remains substantial, with an estimated 50,000 artisanal miners active in the district. However, production records are largely unreported, and the source rocks and fluid pathways remain poorly constrained (Nuwagira et al., 2023).

In summary, gold in Buhweju is hosted in both primary lithologies such as schists and quartzites, and secondary environments including lateritic regolith and stream beds. Artisanal mining activities provide empirical signal of economically recoverable gold, yet the scientific basis for exploration remains underdeveloped.

There is a notable lack of detailed petrographic data to endorse the timing, source, and composition of mineralizing fluids. Furthermore, the spatial distribution of gold anomalies is inadequate, and the interconnection between deep structural controls and surface dispersion is not yet fully established. Most available data instigate from regional surveys and artisanal mining reports, with few systematic investigations conducted at the local scale.

This study therefore aims to address serious gaps in understanding the genesis and distribution of gold deposits in Buhweju. Through the integration of structural mapping, geochemical surveys, and geological fieldwork, the research seeks to:

- Confirm the applicability of the orogenic gold model complete scientific analysis
- Improve the spatial resolution of gold anomaly maps for exploration targeting
- Provide a sustainable framework for mineral development
- Subsidize to Uganda’s mineral resource inventory
- Offer a scientific foundation for policy formulation and investment decisions in the mineral sector

CHAPTER THREE
MATERIALS AND METHODOLOGY

3.1. Materials

This study employed a combination of field equipment, laboratory instruments, and geospatial software to investigate the genesis and spatial distribution of gold deposits in Buhweju District, southwestern Uganda. The materials used were sourced from the Department of Geological Survey and Mines (DGSM) and Department of Geology and Petroleum Studies Makerere University, and were selected to support systematic geological mapping, sampling, and analytical procedures.

Fieldwork was conducted using the following tools and materials:

- GPS receiver for accurate geolocation of sampling sites
- Geological hammer and pickaxe for rock and vein sampling
- Compass clinometer for measuring structural orientations (bedding, foliation, faults)
- Hand lens for in-field mineral identification
- Sample bags and labels for secure sample storage and traceability
- Sieves for processing soil and stream sediment samples
- Geological maps for navigation and lithological referencing.

These instruments made it easier to collect representative samples and record structural characteristics that are necessary to comprehend mineralization of gold deposits. A variety of laboratory techniques were used to analyze the collected samples in order to ascertain their textural properties, mineralogical assemblages, and geochemical composition. These techniques include:

- Inductively Coupled Plasma (ICP) Spectrometry for detecting trace and pathfinder elements.
- Atomic Absorption Spectrometry (AAS) for quantifying gold concentrations
- X-Ray Fluorescence (XRF) for analyzing major oxide compositions
- Light Optical Microscopy for petrographic analysis, including mineral identification and microstructural interpretation

These instruments provided essential data for evaluating the geochemical signatures and confirming the presence of gold and related alteration minerals.

To support spatial analysis and visualization, the following digital platforms were employed:

- Google Earth Pro for satellite imagery interpretation and terrain referencing
- QGIS 3.38.3 (open-source GIS software) for integrating field data, geochemical results, and geological maps to generate geospatial distribution models of gold deposits.

These tools permitted the creation of exploration-ready maps and reinforced the interpretation of structural and lithological controls on mineralization across the study area (figure 3.2).

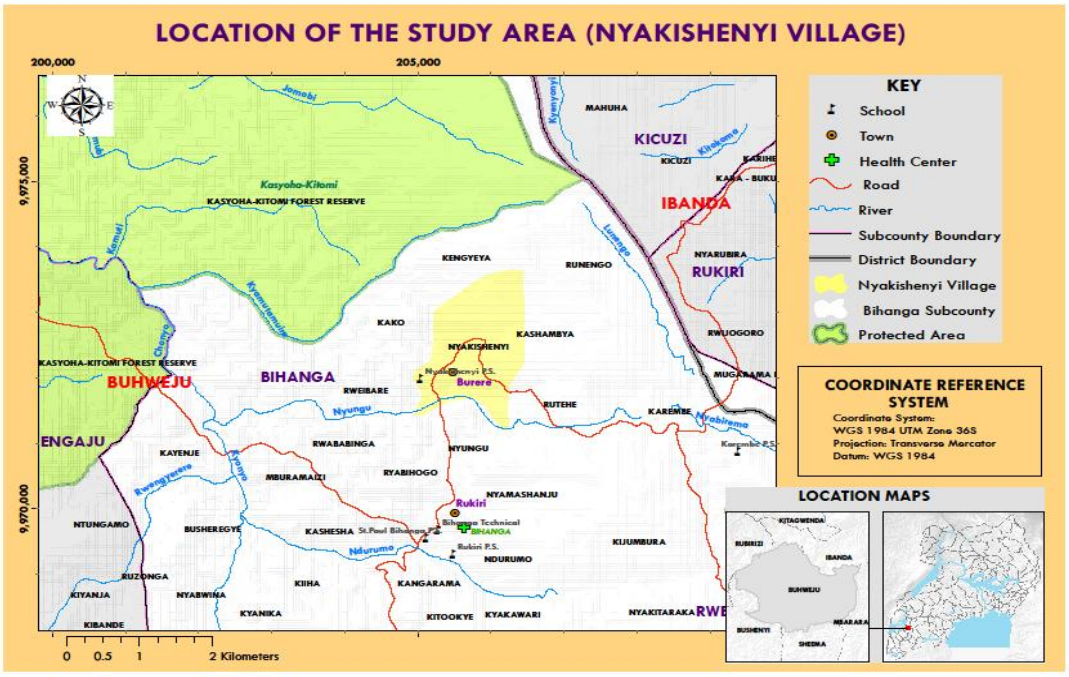

Figure 3.1: *Location map of Buhweju district showing study area (red) within the regional geological context of south western Uganda.*

3.2. Methods

3.2.1. Determination of the geochemical composition in primary and secondary gold ore occurrences

Understanding the mineralizing processes, alteration patterns, and lithological controls in Buhweju District required determination of the geochemical composition of both primary and secondary gold ore occurrences. Systematic geological mapping was piloted and representative samples were taken from regolith habitats and structurally regulated vein systems. The concentrations of major oxides, trace elements, and gold were measured in 50 soil, stream sediment, and rock samples using XRF, ICP-MS, and AAS (Table 3.2).

Active and abandoned artisanal mining pits were mapped and recorded as portion of the geological study in order to attain information of the subsurface geology. In addition to outcrop mapping, these hand dug open pits (figure 4.22) provide valuable natural exposures. A portable GPS device was used to geo-reference each pit, which was included into GIS-based mapping. Pit direction, estimated depth, lithological descriptions, and structural characteristics comprising faults, foliation, and the orientation of quartz veins were among the observations. Geological logging was carried out where safe access was feasible, and representative samples were taken for petrographic and geochemical examination from soil heaps and in situ spotlights. Specific focus was placed on hydrothermal markers, such as quartz veining, iron staining, and alteration zones. These artisanal exposures prominently provided understanding of structural and lithological.

As indicated in Table 3.1, the obtained geochemical datasets were useful in classifying elemental correlations, hydrothermal alteration zones, and geochemical anomalies connected to gold deposits. In order to demonstrate geographical trends and combine geochemical data with lithological and structural aspects, the interpretation process involved geostatistical classification, ternary diagrams, and QGIS-based anomaly mapping. An orogenic gold model was supported by field interpretations of quartzites, schists, and structurally controlled quartz veins, as well as mineralogical indications such as pyrite, arsenopyrite, and alteration halos (silicification, ferruginization, and sericitization).

Table 3.1 *Objectives of geochemical composition for both primary and secondary gold ore occurences.*

Analytical focus	**Target elements/compounds**	**Purpose**
Major Oxides	SiO_2, Al_2O_3, Fe_2O_3, MgO, CaO	Characterize host rock composition and evaluate intensity of hydrothermal alteration
Trace & pathfinder elements	As, Sb, Cu, Pb, Zn, Bi	Detect hydrothermal signatures and delineate geochemical anomalies linked to gold
Gold concentration	Au	Estimate enrichment mechanisms and depositional controls in vein-hosted and regolith-hosted settings

***Table 3.2**: Summary of analytical techniques used in geochemical characterization*

Technique	**Application**	**Principle**	**Justification**
X-Ray Fluorescence (XRF)	Quantification of major oxides (e.g., SiO_2, Al_2O_3, Fe_2O_3)	Detects characteristic secondary X-rays emitted by atoms excited by a primary X-ray source. Each element emits a exclusive energy signature.	Non-destructive and prompt; ideal for bulk rock analysis and alteration mapping in schists and quartzites.
Inductively Coupled Plasma Mass Spectrometry (ICP-MS)	Detection of trace and pathfinder elements (e.g., As, Sb, Cu, Pb, Zn, Bi)	Ionizes samples using high-temperature plasma and splits ions by mass-to-charge ratio; offers ultra-trace sensitivity.	Essential for identifying subtle anomalies and multi-element relations in both primary and secondary ores.
Atomic Absorption Spectrometry (AAS)	Precise quantification of gold concentrations (Au)	Measures absorbance of precise wavelengths of light by free atoms in the gaseous state; follows Beer-Lambert's law.	Highly specific and accurate for gold analysis, particularly in low-grade samples; used with calibration standards.

Major oxides data (TiO_2, AlO_3, FeO, MnO, MgO, CaO, NaO, KO, and PO_5) plotted against SiO_2 (wt %) were used to create harker diagrams in order to assess compositional trends and alteration signatures linked to gold deposits. These diagrams acted as analytical instruments to evaluate the degree of magmatic divergence and hydrothermal alteration among the lithologies sampled.

The geochemical changes that were revealed supported the hypothesis of structurally regulated orogenic gold systems in the Nyakishenyi area and the evolution of the host rocks. The formalization of ASGM operations in Uganda is enabled by this multidisciplinary approach, which also enhances exploration targeting and encourages mining methods that complement national mineral development frameworks.

3.2.1.1. Geochemical sampling

Geochemical sampling was carried out to obtain a comprehensive chemical characterization of both bedrock and surficial materials (soils and sediments) within the study area. (figure3.2) .This approach was essential for identifying geochemical anomalies associated with gold deposits, deducing the elemental distribution relative to lithological units, structural features, and regolith development.

A total of 50 representative samples were collected from both primary gold occurrences containing quartz veins and mineralized host rocks (e.g., schists, quartzites), and secondary gold occurrences such as stream sediments, lateritic soils, and colluvial deposits

Sampling locations were designated basing on lithological variation, structural features such as shear zones and faults, observable artisanal mining activity and presence of hydrothermal alteration zones (e.g., silicification, ferruginization)

The elemental anomalies of gold (Au) and pathfinder elements further indicated mineralized zones. These anomalies were then interpreted in the perspective of host rock composition, structural permeability and fluid pathways, weathering intensity and secondary enrichment processes

This geochemical dataset was significant in understanding the genesis of gold deposits, distinguishing between primary vein-hosted systems and secondary regolith-hosted occurrences hence guiding further exploration targeting.

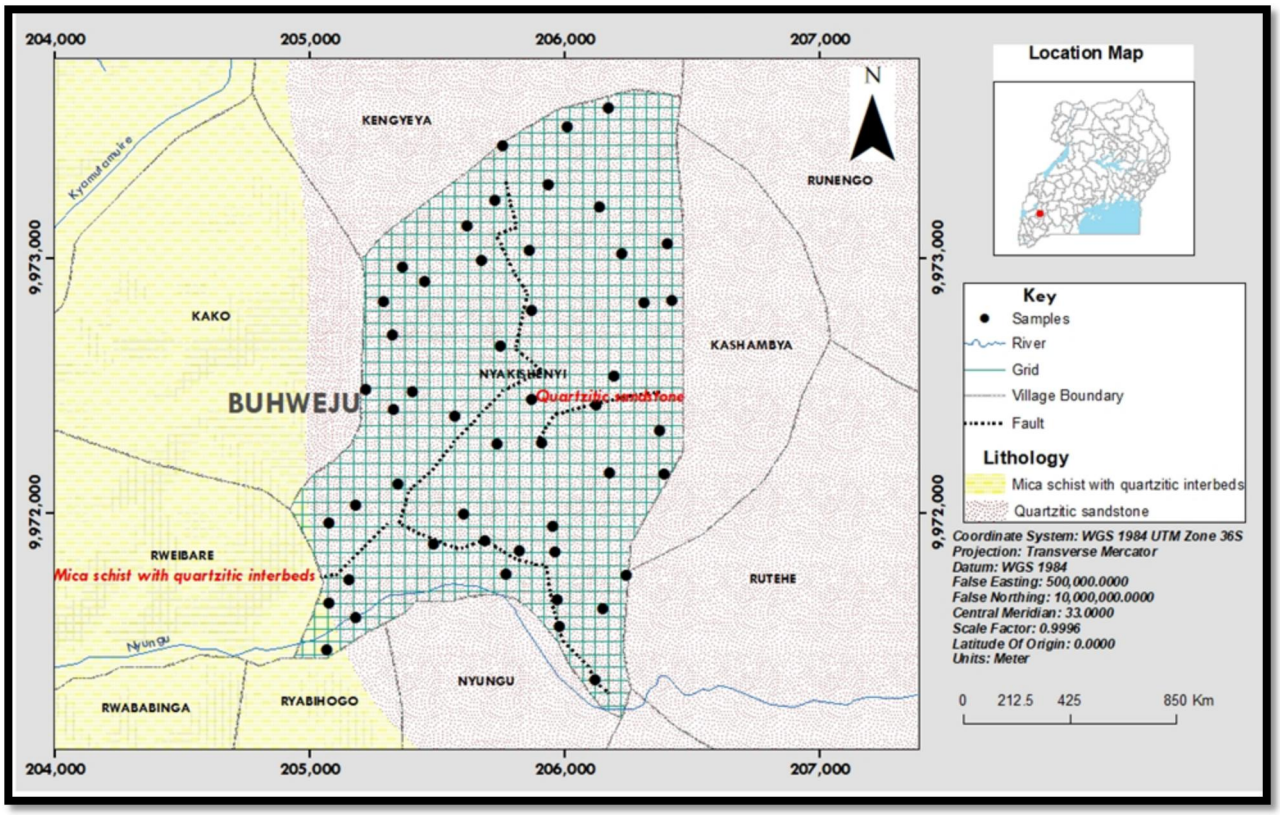

Figure 3.2: *Map showing sampling plan of the study area. The sampling is dominant in quartizitic sandstones, along faults and the trend of the sampling points is in the Nw and Sw. The samples collected include both soil and rocks.*

a) Soil sampling procedure

Soil sampling was conducted on a systematic 100 m × 100 m grid aiming at B-horizon that was selected for its geochemical strength and ability to retain mobile elements. The spacing was based on estimated anomaly sizes from prior surveys. Sampling points were georeferenced using handheld GPS units and physically marked to ensure consistency, spatial uniformity, and reliable geostatistical analysis for anomaly modeling.

Soil samples were collected from the 0–30 cm depth using a hand hoe, targeting the zone most affected by geochemical dispersion while eluding surface organic contamination. Where possible, sampling was done on upslope or mid-slope locations to reduce the effect of transported material and ensure in situ soil representation.

Approximately 2 kg of soil were collected from sampling points and sieved in the field using a 2 mm mesh to obtain fine geochemically active fraction. Samples were stored in labeled Kraft paper bags to avoid moisture retention and microbial alteration. Dependable labeling and detailed field metadata including vegetation, slope, soil characteristics, and proximity to geological features ensured sample integrity and suitability for geochemical analysis targeting gold anomalies and their geological context.

b) Stream sediment sampling

In Nyakishenyi Village, Buhweju District, stream sediment sampling was done as part of the fieldwork to find geochemical signatures linked to potential gold deposits. This approach was selected because it provides a dependable but indirect way to track upstream mineral sources in areas with dense vegetation cover and little exposure to bedrock.

Sampling locations were identified through a review of drainage networks using topographic maps and satellite imagery. Priority was given to streams intersecting suspected mineralized zones, including areas with mapped quartz veins, shear zones, and artisanal mining activity. Both first-order and second-order streams were considered, with caution taken to ensure a spatially distributed sampling grid across the study area.

A total of 20 stream sediment samples were collected, with 10 samples focused on first-order streams and 10 samples from second-order streams. This balanced approach allowed for both localized anomaly detection and broader catchment-scale geochemical screening.

At each selected stream point, sediment samples were collected from active channels (Figure 3-3). Fine-grained materials particularly silt and clay fractions were targeted using a clean plastic scoop or trowel. These fractions were preferentially sampled because they are more geochemically reactive and capable of adsorbing and transporting metal ions such as gold. Point bars, riffles, and areas behind boulders were specifically chosen as sampling sites

because they act as natural traps where suspended sediments settle, concentrating fine particles and enhancing the likelihood of detecting upstream geochemical anomalies.

Within a 5–10 m section of the stream, sediments were composited from many locations (usually 3–5 m apart) to guarantee sample representativeness. Five kilograms of sediments were gathered at each location and promptly placed in sterile and properly labeled sample bags (Figure 3-5). A portable GPS device was used to record the sampling locations in order to guarantee precise georeferencing for future mapping and analysis.

All samples were dried in an oven for 24 hours and stored to prevent contamination or degradation. Sampling tools were rinsed thoroughly between sites to avoid cross-contamination. Upon completion of fieldwork, all specimens were transported to the base station for further preparation and storage prior to laboratory submission.

This method provided a valuable dataset for identifying downstream geochemical anomalies, which were later interpreted in relation to local lithology, structural controls, and mineralization patterns within the study area.

Figure 3.3: *Photos showing soil stream sediment sampling in the water channel within the study area. The samples obtained include sediments with clay and silt. This water stream is located in the valley near the mining areas.*

c) Rock sampling procedure

Rock sampling was conducted to collect fresh, un weathered specimens from outcrops that were geologically representative of the lithological units identified during field mapping (Figure 3-4). Particular emphasis was placed on sampling quartz veins, schists, and altered zones associated with potential hydrothermal activity, as these lithologies are known to host auriferous mineralization within the Buhweju–Mashonga gold district.

To ensure sample representativeness, each specimen was extracted from a homogeneous portion of the outcrop, avoiding weathered surfaces. Surface material was chipped away using a geological hammer, and fresh rock was exposed and collected. Each sample weighed approximately 4–5kgs, providing sufficient material for laboratory analysis, including duplicate testing.

Rock fragments were placed into polythene sample bags and labeled using permanent waterproof markers. Each label included a unique sample identification code, brief lithological description, and coordinates recorded using a handheld GPS device with ±3 m accuracy.

In addition to labeling, detailed field notes were recorded for each sample, including observations on texture and mineralogy, structural orientation (e.g., foliation, vein trend), and visible alteration features. These included: Silicification, particularly in quartz veins and silicified shale units, indicating silica-rich hydrothermal fluid activity. Oxidation and hematization, observed as reddish staining and iron oxide coatings, suggested supergene alteration and weathering of sulfide minerals. Sulfide-pyritization, marked by disseminated or vein-hosted pyrite, often associated with gold mineralization in schistose and quartzitic host rocks.

In order to characterize the gold-bearing systems in the study area, this process ensured rock samples were geologically significant, well-documented, and appropriate for further petrographic, geochemical, and mineralogical examination.

Figure 3.4: *Photo indicating fragments of rock sample from outcrop of schist in the study area.*

d) Sample preparation and laboratory analysis.

A total of 50 samples, consisting soils, stream sediments, and rock specimens, were sent to the Department of Geological Survey (DGS), Entebbe for geochemical analysis. These samples were collected from both primary and secondary gold occurrences from the study area to identify geochemical composition.

Standard sample preparation procedures were followed to ensure analytical consistency and precision. Each sample was air-dried to remove moisture, pulverized to ensure homogenization, and sieved to <75 μm and obtained fine fraction suitable for geochemical analysis.

Prepared samples were analyzed using Inductively Coupled Plasma Mass Spectrometry (ICP-MS) for high-sensitivity detection of trace and pathfinder elements, X-Ray Fluorescence (XRF) for quantification of major oxides and selected trace elements.

The analytical suite included

- Major oxides: SiO_2, Al_2O_3, Fe_2O_3, MnO, MgO, CaO, Na_2O, K_2O, P_2O_5 and these oxides were used to characterize host rock composition and detect hydrothermal alteration zones associated with gold deposits.
- Transition metals such as Cu, Zn and V associated with sulfide deposits and polymetallic veins that may co-occur with gold deposits in hydrothermal systems.
- Lithophile elements included Zr, Y, Th which served as immobile geochemical markers for lithological discrimination and felsic source identification.
- Gold, pathfinder and associated trace elements such as Ag, As, B, Ce, Co, Cr, Cu, Hg, Hf, Mo, Ni, Pb, Rb, Sb, Sc, Sn, Sr, Ta, Th, U, V, W, Y, Zn, Z were critical for delineating geochemical halos and tracing mineralizing fluids. Elements such as As, Sb, Hg, and Mo are well-established pathfinders in orogenic gold systems, while Ag, Pb, and Cu may indicate polymetallic associations. Their spatial distribution supports anomaly modeling and enhances the interpretation of gold enrichment mechanisms.

The genetic model of orogenic gold deposits in Buhweju District was supported by these geochemical datasets, which played a critical role in determining elemental anomalies associated with gold deposits, mineral associations, and analyzing alteration patterns across lithological units in relation to structural controls, regolith development, and hydrothermal fluid pathways.

3.2.1.2. Quality control procedures

Throughout sampling, preparation and analysis process, QA/QC framework was used for precision and consistency of the geochemical dataset. Field procedures such as avoiding sample contamination, collecting field duplicates systematically (every fifth soil sample), and calibrating were ensured through use of Certified Reference Materials (CRMs). Field instruments were cleaned in between locations and samples were kept in containers that were clearly marked and kept apart to avoid cross-contamination. GPS-referenced metadata and thorough field notes were documented to improve traceability and contextual interpretation.

QA/QC procedures were observed in the laboratory by use of certified standards to every analytical batch, blanks and random duplicates for stream sediment samples to ensure

accuracy and identify instrumental drift. The anomalous results were cross-validated using several methods to maintain robustness of the data .Combining these methods, the geochemical data were guaranteed to be accurate, repeatable, and appropriate for detecting elemental abnormalities and supporting the genetic interpretation of gold mineralization in Buhweju District.

Figure 3.5: *showing samples (rock, soil, stream sediments) in well packed material as caution for quality control as the samples were assembled at the Laboratory to undergo sample preparation at mineral dressing lab then after be taken for analysis.*

3.2.2 Characterization of gold deposits in Buhweju.

The characterization of gold deposits in Buhweju District was done through use of a multidisciplinary approach that combined detailed geological mapping, structural analysis, and mineralogical assessment. This approach aimed at understanding the spatial distribution, genesis, and host rock relationships of gold deposits' occurrences within Nyakashenyi area.

Geological mapping was conducted at a scale of 1:10,000, focusing on lithological units identification (quartzites, schists, phyllites, and granitoids), alteration zones, quartz veins, and artisanal mining sites. Field observations included visual assessment of outcrops based on texture, mineralogy, weathering patterns, and structural features. Representative samples were collected for petrographic analysis under polarized light microscopy (PPL and XPL),

enabling precise determination of mineral associations linked to gold deposits. Quartz veins hosting visible sulfides and alteration halos were marked by silicification, ferruginization, and sericitization were prioritized, with accessory minerals such as pyrite, arsenopyrite, and chlorite which serve as indicators of hydrothermal processes.

Structural mapping was a significant component of the study which aimed at delineating orientation, distribution, and key deformation features such as faults, joints, folds, foliations, and shear zones. These features influenced the geometry of host rocks that act as conduits or traps for hydrothermal fluids responsible for gold mobilization and deposition. Field measurements were taken using a Brunton compass and GPS device, and structural data were plotted on a base map to show spatial trends. Rose diagrams and stereonets were constructed to analyze the orientation and kinematics of structural features in relation to gold-bearing zones. Special attention was given to northeast–southwest (NE–SW) and northwest–southeast (NW–SE) striking lineaments that are regionally recognized as significant controls on gold emplacement.

Foliation planes, schistosity in metamorphic rocks, iron-stained fractures and joints, quartz infill, and clay alteration were the main subjects of field observations. These features are indicative of the movement of hydrothermal fluids, faults and shear zones which can be identified by offset features, gouge material, alteration halos, folds, and kink bands at lithological contacts or vein intersections.

Interpreting the tectonic history of the Buhweju–Mashonga gold district and creating a genetic model for the gold deposits in Nyakashenyi required structural analysis. The combination of mineralogical, structural, and geological data offered a framework for understanding distribution of gold and directing exploration techniques in the region.

3.2.3 Mapping spatial distribution of geological features in the area

Detailed geological mapping was conducted throughout the study area to document various features such as lithologies, structural elements, and their spatial relationships. The field survey involved recording locations of outcrops, alteration zones, and artisanal mining sites using GPS for accurate spatial referencing.

Structural data such as fault orientations, shear zones, joints, and folds were measured using a compass, and stereonet diagrams were plotted to visualize their geometric relationships. Observational data from mining sites were integrated to infer subsurface lithological and structural patterns.

The collected field data were combined with geochemical analyses and GIS datasets to generate comprehensive maps illustrating the spatial distribution of lithological units, structural controls, and zones of mineralization. This integrative approach provided a robust framework for understanding the geological architecture and its influence on gold occurrence within the study area.

3.2.3.1 Geological mapping

Detailed geological mapping was carried out within the study area .Different lithology such as quartz, schists and sandstones and several geological features included beds, shear zones, joints, fractures and water channels. Equipments used during field mapping included compass, GPS, notebook and pen. Observations were recorded alongside their coordinates for easy follow-up during advanced exploration.

3.2.3.2 Observational study on artisanal mining sites.

As part of the field-based geological investigation, systematic mapping and documentation of artisanal mining pits were undertaken. These pits, manually excavated by local miners, offered natural exposures of subsurface geology and served as supplementary observation points.

The study commenced with field reconnaissance to identify both active and abandoned artisanal sites within the study area. Once located, pits were geo-referenced using a handheld GPS device, and data was recorded for integration into GIS-based mapping.

At each site, observations included measurements of pit orientation, estimated depth, and dimensions, along with detailed descriptions of lithological units exposed along the pit walls. Where safe access was possible, geological logging was conducted on the exposed sections, documenting lithological contacts, vein orientations, and structural features such as foliation and fault traces.

Special attention was given to quartz veins and associated alteration zones especially where there was discoloration which indicated potential hydrothermal activity. Photographic documentation of each pit was done to support field records and facilitate analysis later.

Representative samples were collected from in situ exposures and, where applicable, from soil heaps for geochemical analysis. The mapping of artisanal pits was integrated into the broader geological mapping framework that provided insight into subsurface conditions often obscured by vegetation and soil cover. This method made a contribution to a thorough comprehension of the structural and lithological links throughout the study area.

CHAPTER FOUR
PRESENTATION OF RESULTS

4.1 Geochemical Composition in Primary and Secondary Gold Ore Occurrences

Geochemical analysis of rock, soil, and stream sediment samples from the Buhweju area revealed major and trace elements associated with gold mineralization. Major oxides (SiO_2, Al_2O_3, Fe_2O_3, TiO_2, CaO, MgO, K_2O, Na_2O, MnO) reflect lithological composition, weathering intensity, and mineralization potential. Trace elements including As, Sb, Cu, W, Pb, Zn, Th, U, Zr, Sr, V, Cr, and Y provide insights into hydrothermal alteration, polymetallic sulfide systems, and lithological provenance**.**

4.1.1 Major Oxide Composition

SiO_2 concentrations (70–79 wt.%) confirm quartz-rich lithologies (quartzites, schists). Moderately elevated Fe_2O_3 (5–7 wt.%) and Al_2O_3 (10–12 wt.%) indicate iron-rich alteration zones and intense weathering, consistent with hydrothermal systems. MgO and CaO are low, reflecting advanced leaching typical of tropical terrains. TiO_2 and immobile elements (Zr, Y) suggest residual enrichment linked to magmatic/metamorphic sources.

Figures 4.1–4.2 show systematic oxide variation relative to SiO_2. Ferromagnesian oxides decline with silica, while K_2O enrichment indicates evolved felsic compositions. These patterns support fractional crystallization, felsic differentiation, and structurally controlled orogenic gold systems**.**

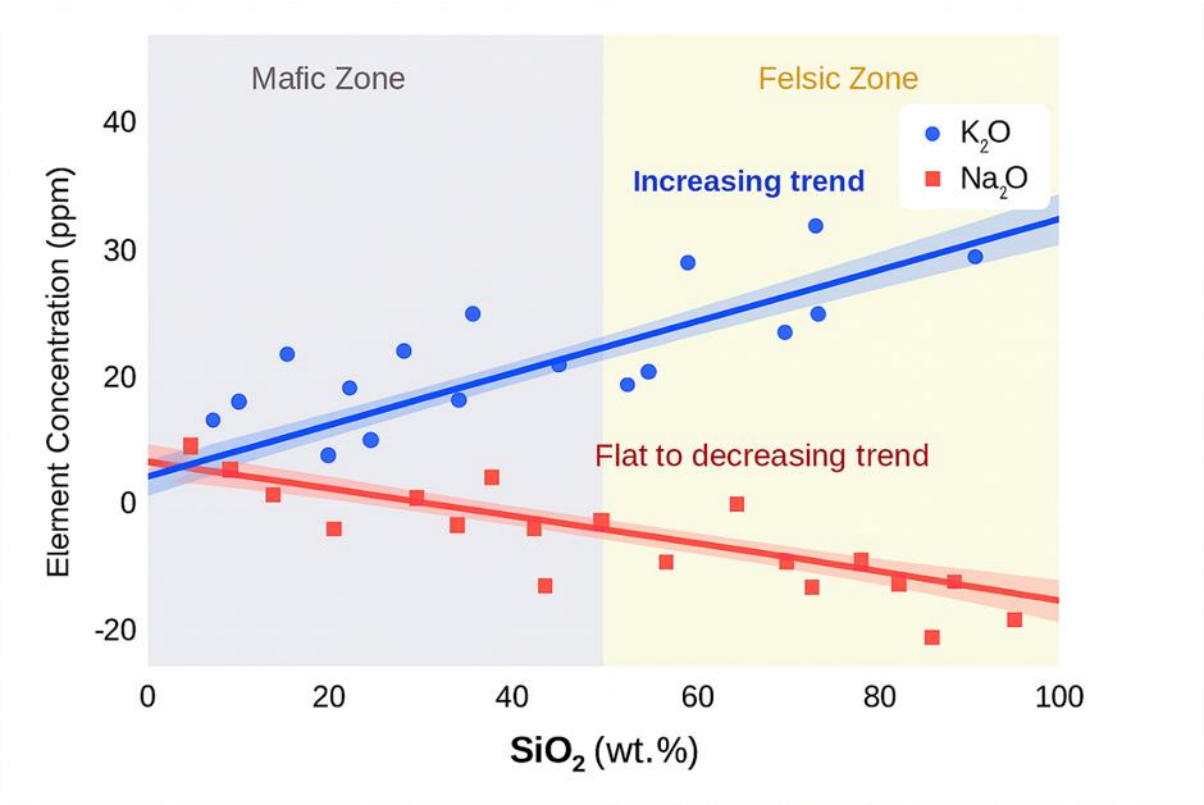

Figure 4.1: *Harker diagram showing major oxide variation with SiO_2 in Nyakishenyi rock samples. Declining MgO, Fe_2O_3, CaO, TiO_2, and MnO with increasing silica reflects mafic mineral compatibility, while enrichment of K_2O indicates evolved felsic compositions. Scale bar = wt. % oxide concentration.*

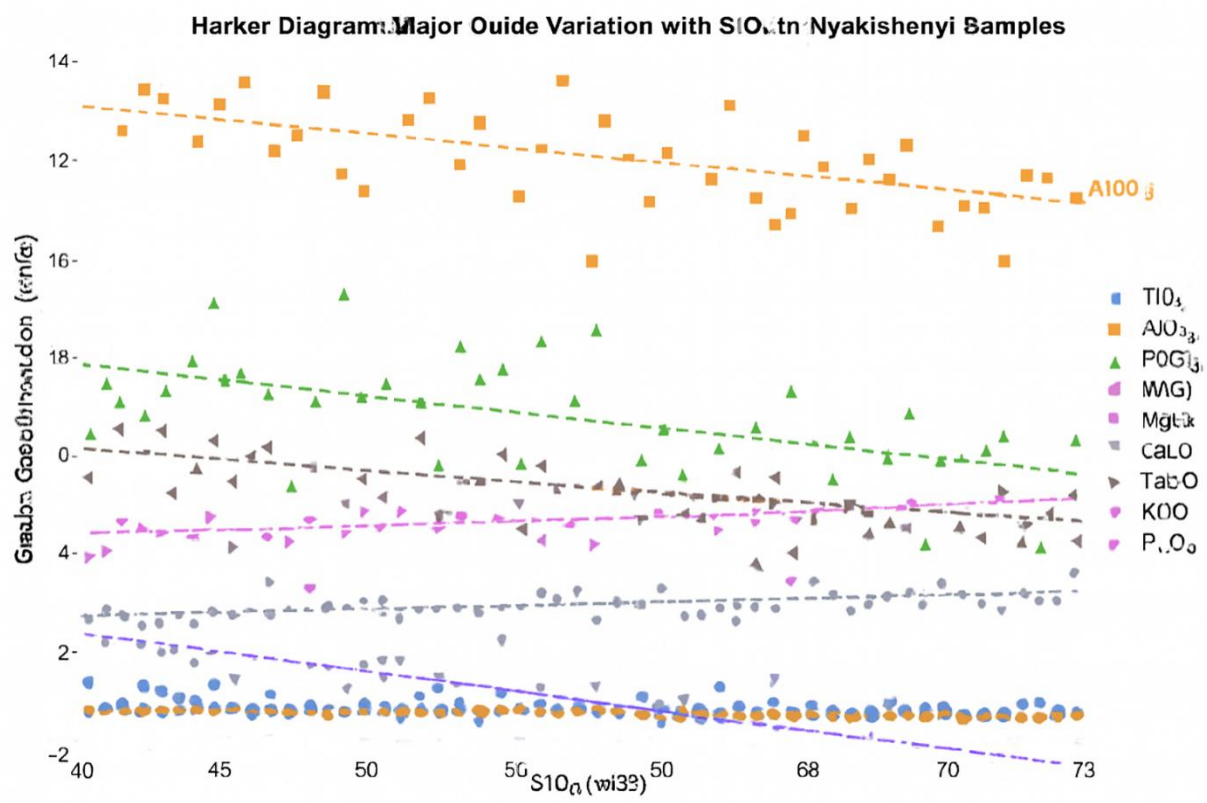

***Figure 4.2**: Harker diagram of principal oxides vs. SiO_2 in Nyakishenyi samples. Systematic decline of ferromagnesian oxides contrasts with enrichment of K_2O, consistent with magmatic differentiation and hydrothermal alteration. Scale bar = wt. % oxide concentration.*

4.1.2 Trace and Rare Element Signatures

***Table 4.1:** Trace element concentrations and exploration significance in Nyakishenyi samples.*

Element	Range (ppm)	Mean (ppm)	Exploration significance
As	≤ 6.3	3.2	Strong Au correlation; key pathfinder (arsenopyrite)
Sb	0.3–0.7	0.5	Hydrothermal indicator; supports As anomalies
Cu	35–97	66	Polymetallic association; alteration halos near intrusives
W	0.8–0.97	0.9	High-temperature hydrothermal indicator (scheelite)
Pb	40–68	54	Galena association; polymetallic sulfide zones

Zn	90–110	100	Polymetallic halo; alteration zone marker
Th	4.3–5.4	4.8	Granitic–metamorphic provenance
U	2.1–3.7	2.9	Lithophile; supports tectonic context
Zr	143–200	172	Immobile; felsic provenance, residual halos
Sr	280–350	315	Mobile; alteration mapping
V	104–122	113	Mafic component indicator
Cr	150–200	175	Mafic provenance marker
Y	86–110	98	Lateritic environment indicator

Figures 4.3–4.4 highlight pathfinder associations. Au–As correlation (r = 0.77) confirms arsenopyrite as a key host mineral; Au–Sb (r = 0.52) supports stibnite association. Cu and Zn show polymetallic halo effects, while Pb indicates galena presence but weak predictive value.

s

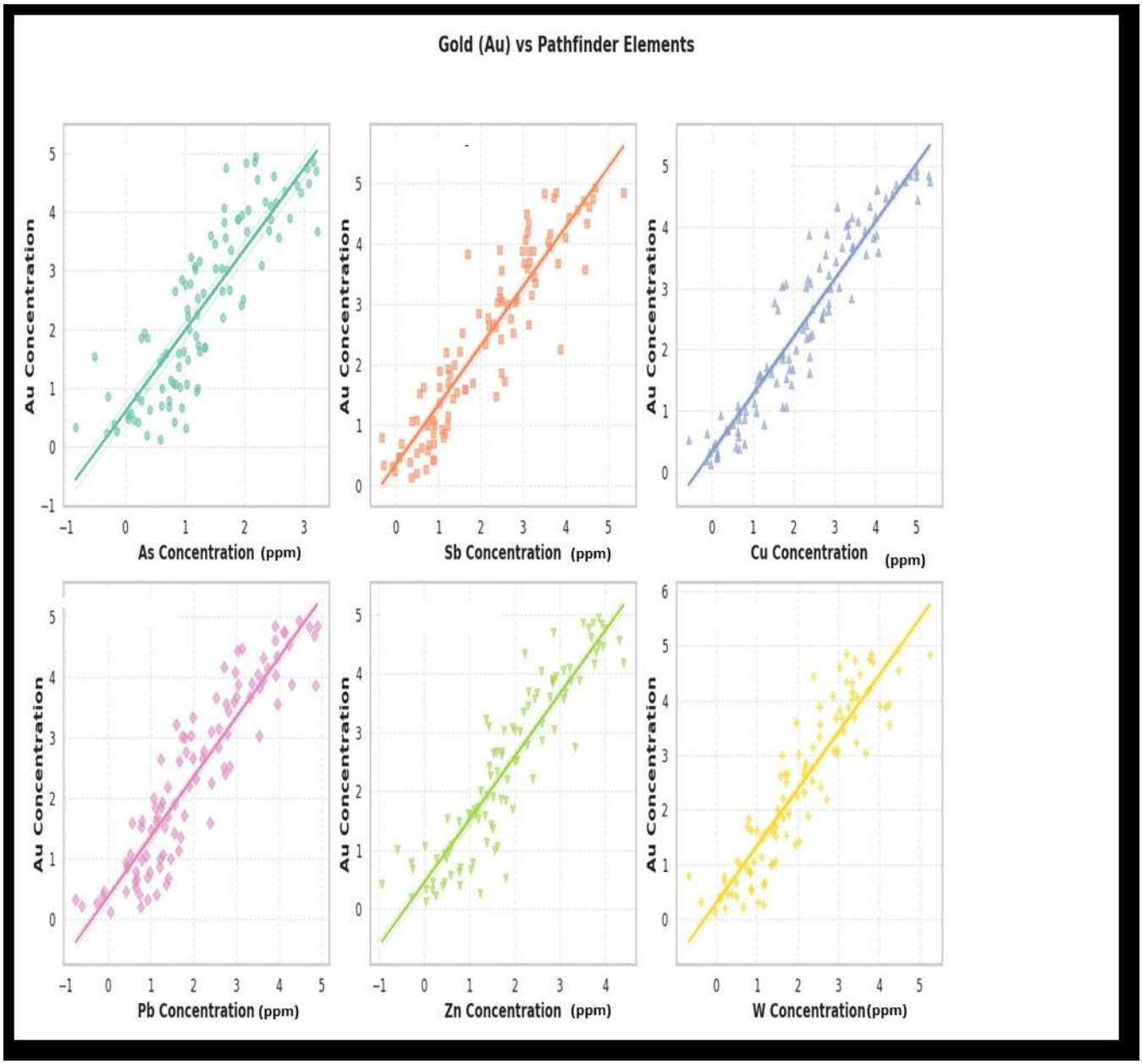

Figure 4.3*: Scatter plot of Au vs. pathfinder elements (As, Sb, Cu, Pb, Zn, W). Strong Au–As correlation confirms arsenopyrite as a key host mineral; moderate Au–Sb supports stibnite association. Cu and Zn indicate polymetallic halos. Scale bar = 1 ppm Au.*

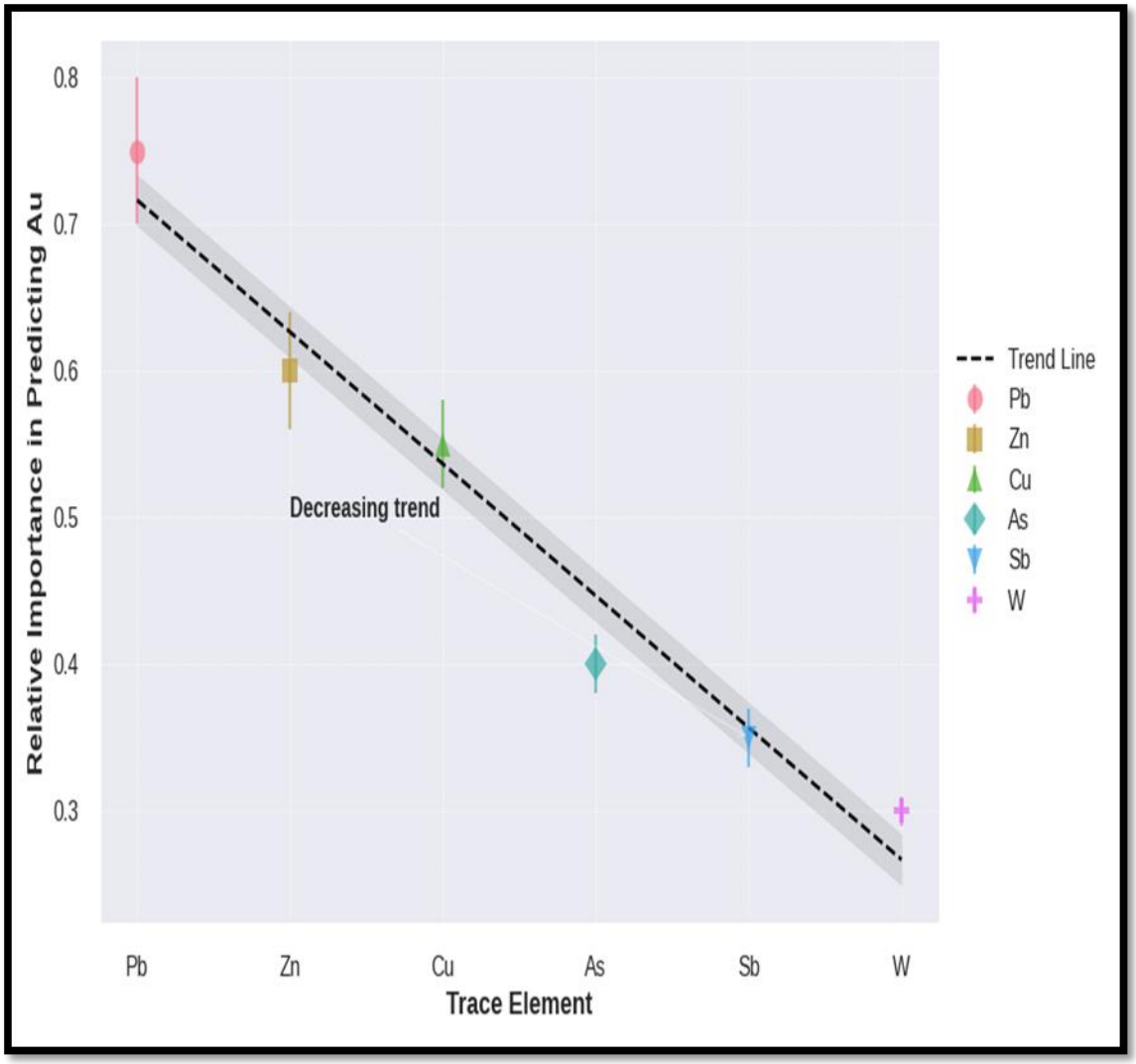

Figure 4.4: *Horizontal bar chart ranking trace elements by predictive relevance to Au concentration. Pb shows strongest association, followed by Zn and Cu, while As and Sb act as classic pathfinders. W reflects deeper hydrothermal processes. Scale bar = ppm concentration.*

Table 4.2: Pearson correlation coefficients between Au and selected trace elements.

Element Pair	r Value	Interpretation	
Au–As	0.77	Strong correlation; arsenopyrite key host	
Au–Sb	0.52	Moderate; stibnite association	
Au–W	0.43	Weak–moderate; scheelite/wolframite possible	

Au–Cu	0.02	Very weak; background alteration	
Au–Zn	0.03	Very weak; dispersed sulfides	
Au–Pb	0.18	Weak; galena present but not predictive	

4.1.3 Elemental associations and gold indicator potential

Residual enrichment zones (Ti, Zr, Y with high SiO_2) indicate immobile geochemical footprints favorable for exploration in lateritic terrains. Slight enrichment of W, Cu, Zn reflects hydrothermal alteration along shear zones and faults. Au anomalies spatially align with As and Sb, confirming structurally controlled orogenic systems.

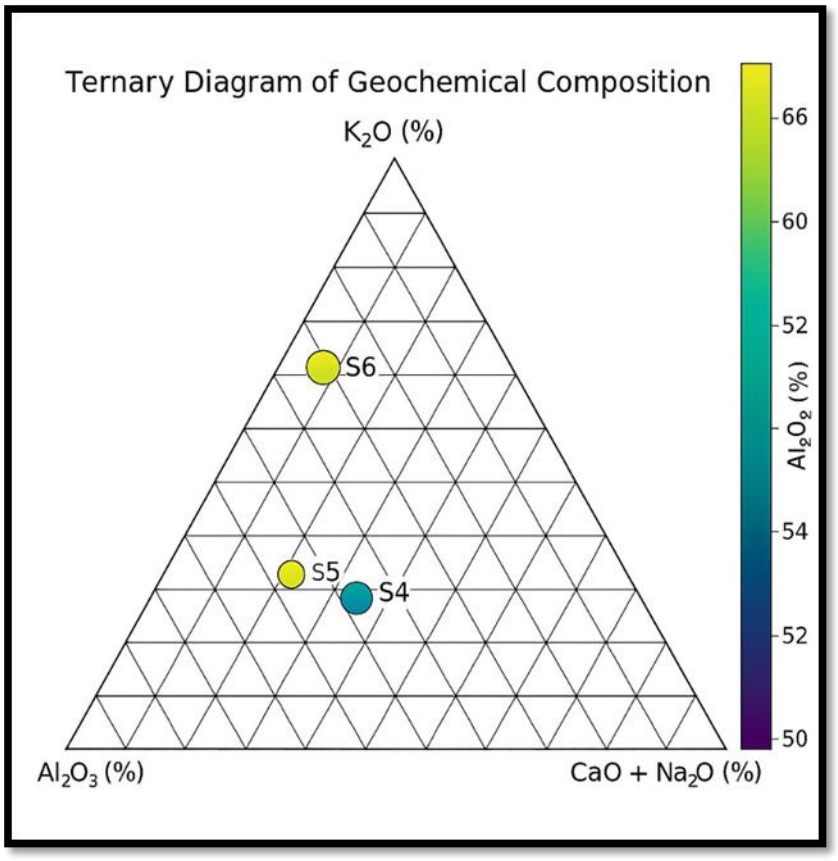

***Figure 4.5**: Ternary diagram of (CaO + Na_2O), K_2O, and Al_2O_3 in Nyakishenyi samples. Gold‑rich samples cluster near the K_2O corner, indicating potassic alteration typical of*

hydrothermal systems. High Al_2O_3 suggests argillic alteration. Scale bar = wt.% oxide concentration.

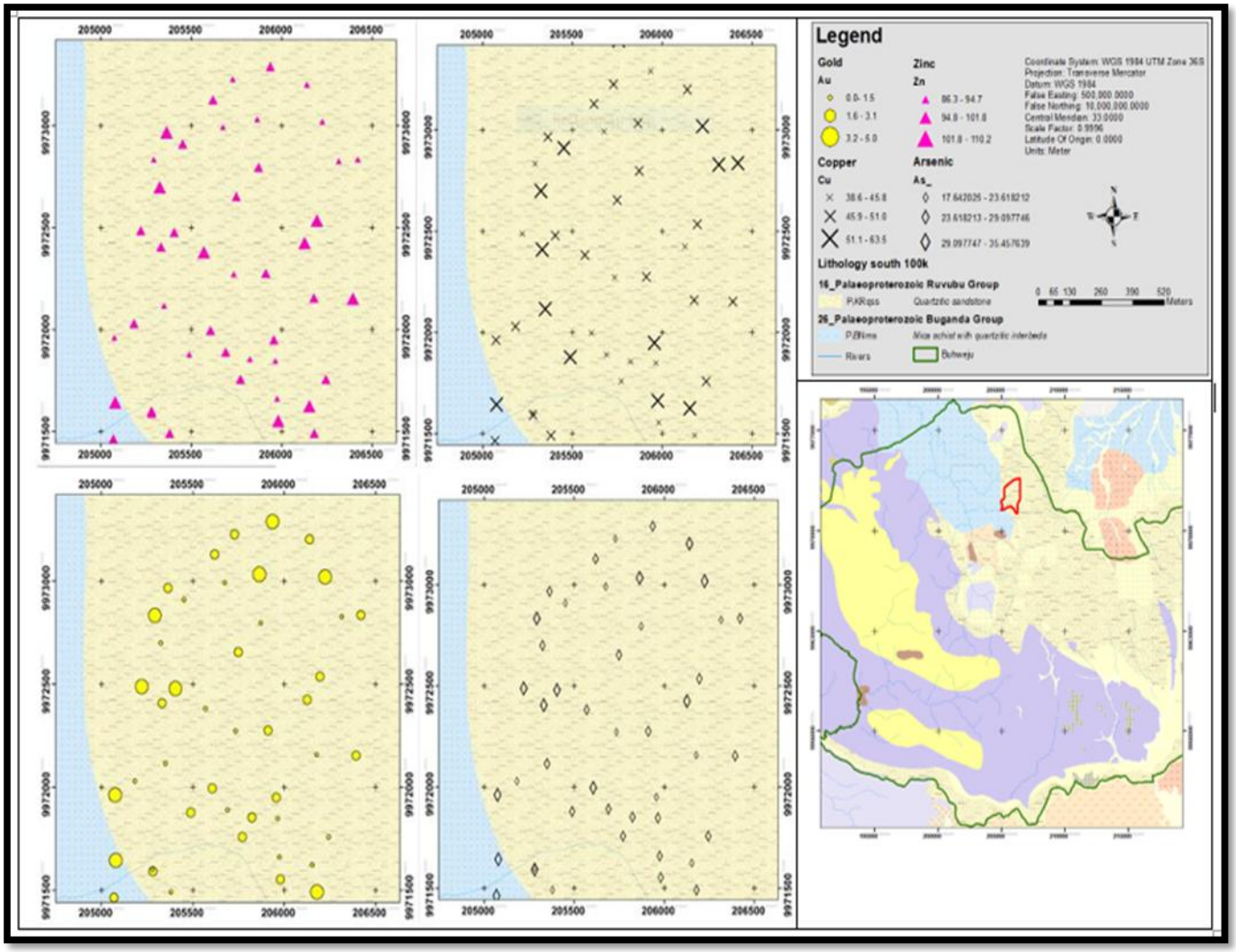

***Figure 4.6**: Geochemical distribution map of Au, Ag, Cu, Zn, and As anomalies in Nyakishenyi. Elevated Au and As align with mica schist units and artisanal mining sites, confirming structurally controlled mineralization. Cu and Zn anomalies are scattered, reflecting polymetallic dispersion. Map includes scale bar = 1 km.*

4.1.4 Comparison of primary and secondary gold occurrences

***Table 4.3:** Geochemical composition of primary gold occurrences.*

Element	Range (ppm / wt.%)	Mean	Exploration Significance

Au (ppm)	1.2–8.7	4.3	High-grade vein mineralization
As (ppm)	40–320	140	Arsenopyrite pathfinder
Cu (ppm)	30–160	90	Hydrothermal alteration
Pb (ppm)	12–105	65	Galena association
Zn (ppm)	25–180	82	Minor sulfide halo
Fe_2O_3 (wt.%)	4.8–11.2	7.5	Pyritization indicator
SiO_2 (wt.%)	65–91	78	Quartz-rich lithologies

***Table 4.4**: Geochemical composition of secondary gold occurrences.*

Element	**Range (ppm / wt.%)**	**Mean**	**Geological significance**
Au (ppm)	0.2–3.4	1.1	Placer enrichment
Fe_2O_3 (wt.%)	3.5–8.1	5.9	Lateritic profile
Al_2O_3 (wt.%)	12–26	18.4	Kaolinitic clays
SiO_2 (wt.%)	48–72	60.3	Clay + quartz detritus
As, Cu, Pb (ppm) –			Leached during weathering

Primary ores (quartz veins in schists) show elevated Au (mean 4.3 ppm) with strong As, Cu, Pb, Zn associations, confirming hydrothermal origin. Secondary ores (soils, alluvials) show lower Au (mean 1.1 ppm) and depletion of pathfinders due to tropical weathering, reflecting residual enrichment. These contrasts delineate zones of preserved hydrothermal signatures versus secondary dispersion, guiding exploration strategies.

4.2 Characterization of Gold Deposits in Nyakishenyi Village

4.2.1 Field characterization

Gold mineralization in Nyakishenyi occurs within milky white to grey quartz veins hosted in schist and gneiss. These veins, ranging from 0.5–50 cm thick, consistently trend NW–SE and dip steeply (60–85°). As shown in Figure 4.7, the veins display iron staining, gossan textures, and brecciation, confirming oxidation and sulfide weathering. The hammer reference in Figures 4.7A–B provides scale, highlighting vein orientation and fracture depth. Brecciated textures (Figure 4.7C) and sharp vein contacts (Figure 4.7D) illustrate brittle deformation and late-stage fluid influx, supporting a structurally controlled orogenic gold system.

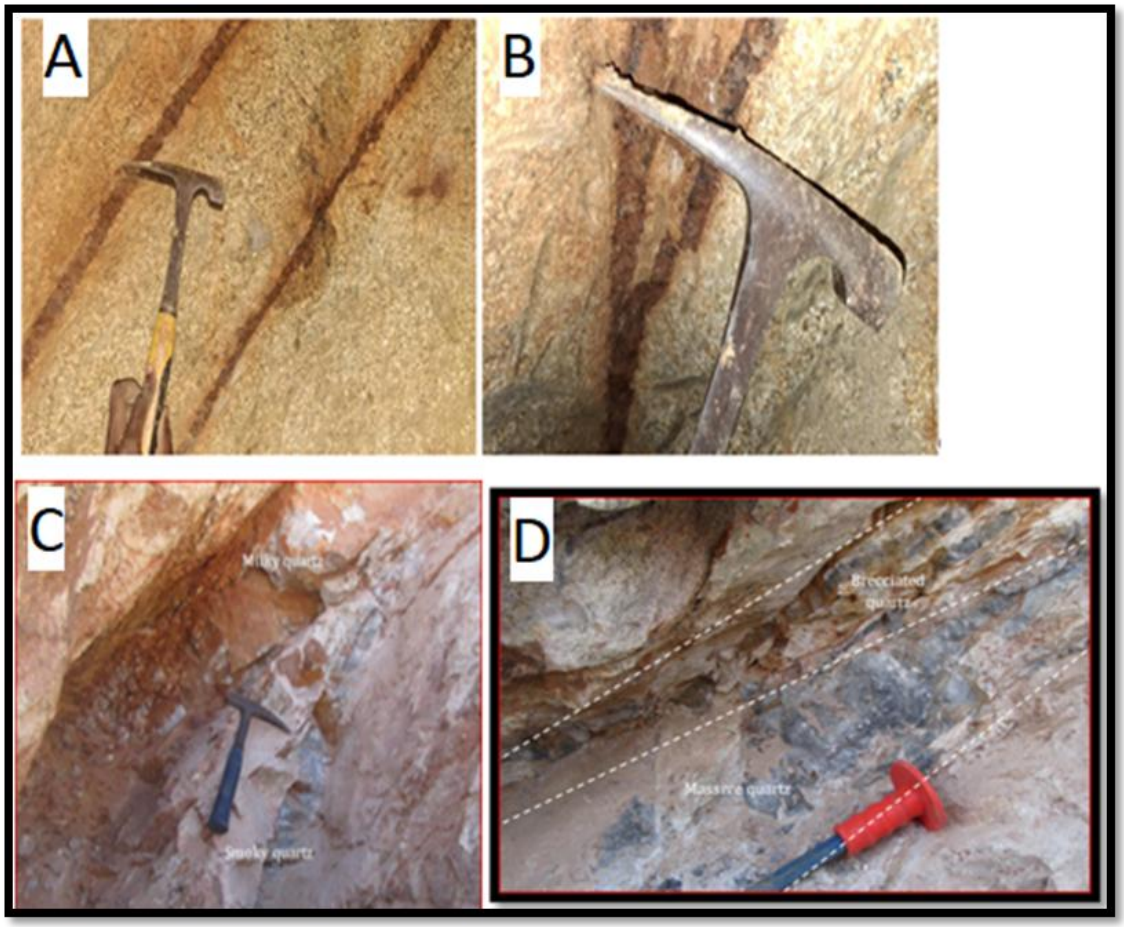

Figure 4.7 (A–D)*: Gold-bearing quartz veins hosted in foliated schist and gneiss at Nyakishenyi, aligned along NW–SE–trending shear zones, indicating strong structural control and an orogenic-style gold mineralization system.*

4.2.2 Petrographic observations

a) Quartzites

Table 4.5: *Petrographic characteristics of quartz from gold-bearing veins in Nyakishenyi*

Feature	**Description**
Texture	Medium–coarse grained, granoblastic, non-foliated anhedral quartz (2–4 mm)
Quartz (PPL)	Colorless, translucent, low relief
Quartz (XPL)	First-order gray–white interference colors; undulose extinction
Deformation Features	Undulose extinction indicating tectonic stress related to shear zones
Microstructures	Microfractures and secondary quartz veinlets with iron oxides
Alteration	Sericite–chlorite halos with minor sulphides around gold-bearing veins

Thin-section analysis reveals medium to coarse-grained quartz with granoblastic textures. Under PPL, quartz appears translucent and colorless, while under XPL it shows undulose extinction, indicating recrystallization under tectonic stress. Microfractures filled with secondary quartz and iron oxides are visible, with alteration halos of sericite and chlorite. These features, summarized in Table 4.5, confirm brittle deformation and hydrothermal fluid pathways.

b) Schists

Petrographic analysis of schist samples (Table 4.6) reveals a plagioclase-dominated assemblage with biotite and muscovite undergoing chlorite–sericite alteration, while trace pyrite occurs along foliation planes and microfractures, indicating structurally controlled hydrothermal fluid flow associated with gold mineralization.

Table 4.6: *Petrographic characteristics of schist from Nyakishenyi Village showing mineral assemblage, optical properties, modal abundance, and alteration features relevant to structurally controlled gold mineralization***.**

Mineral	PPL Characteristics	Xpl characteristics	Modal Abundance	Interpretive Features
Biotite (Bt	Brown, pleochroic, prismatic	Strong birefringence; bird's-eye extinction	~2%	insdicating hydrothermal alteration
Muscovite (Ms)	Colorless, flaky to fan-shaped	Second-order interference colors	~1%	Associated with calcite and chlorite; reflects sericitic alteration near veins
Plagioclase (Plg)	Colorless, prismatic, moderate relief	Lamellar twinning; extinction angles 10°–15° (An10–An30)	~35%	Dominant feldspar phase; locally altered adjacent to mineralized zones
Pyrite (FeS_2)	Bright yellow, high relief, cubic	Isotropic (low-order colors)	Trace	Occurs along foliation and microfractures; commonly oxidized, indicating sulphide-related gold association

4.2.3 Alteration and mineralization features

Petrographic analysis reveals systematic alteration and deformation features closely associated with gold-bearing structures in Nyakishenyi. Sericitization and chloritization are strongly developed along quartz vein margins and foliation planes, indicating sustained hydrothermal fluid flow along structurally controlled permeability pathways (Figure 4.8D). These alteration assemblages reflect fluid–rock interaction under greenschist-facies conditions typical of orogenic gold systems.

Sulphide mineralization is dominated by pyrite, which occurs as disseminated grains and along microfractures, commonly associated with iron oxide staining and secondary mica

growth. The spatial association of pyrite with alteration halos suggests sulphide deposition during hydrothermal fluid circulation, with subsequent oxidation during weathering.

Mylonitic fabrics are well developed within the host schist and quartz-rich zones, characterized by grain-size reduction, quartz ribboning, and alignment of mica aggregates (Figures 4.8A, 4.8D). These features confirm ductile deformation within shear zones and indicate that gold mineralization was structurally controlled and synchronous with deformation.

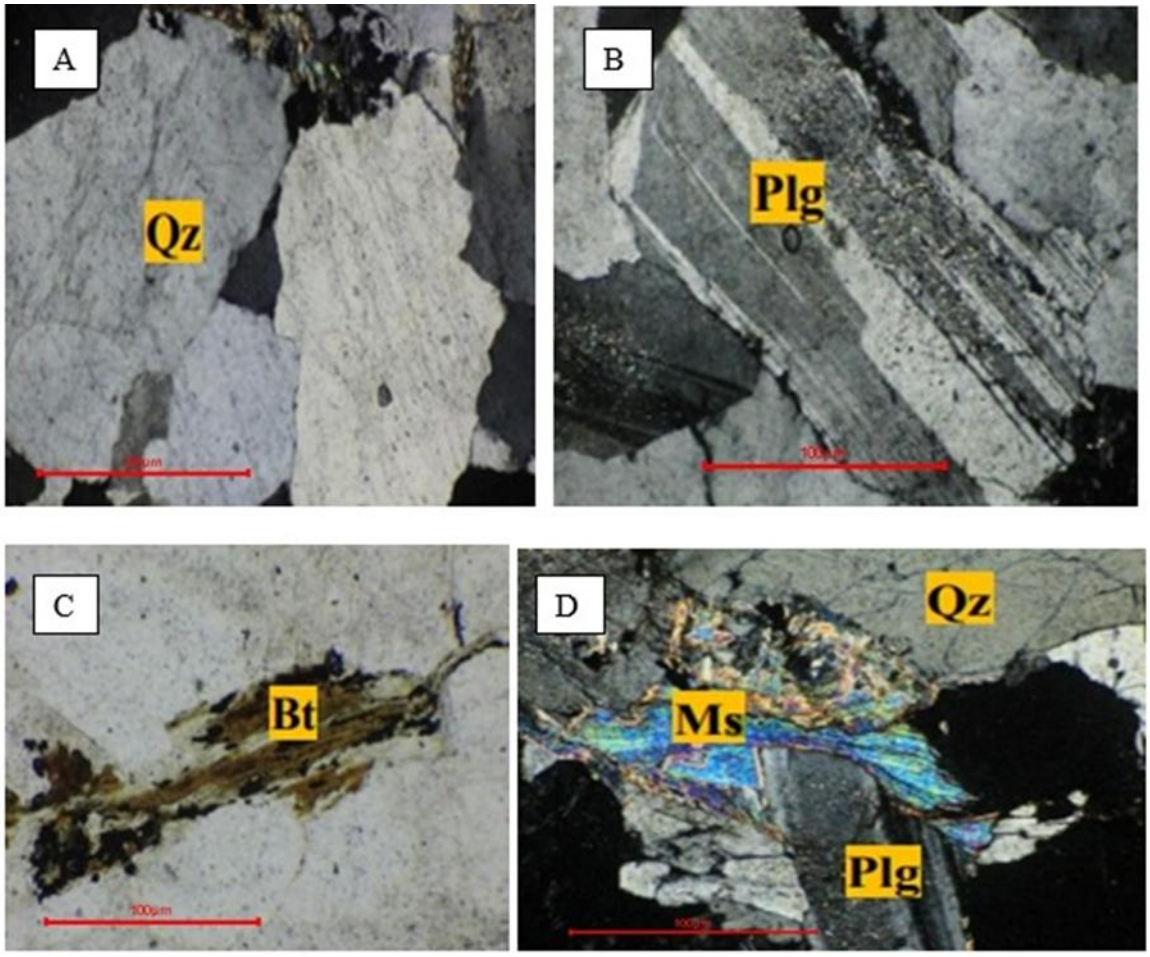

Figure 4.8 (A–D) *:shows (A) Recrystallized quartz represents deformation-related strain; (B) twinned plagioclase and (C) pleochroic biotite represent primary mineral assemblages.(D) Muscovite represents sericitic alteration linked to hydrothermal fluids.*

4.2.4.Ore petrography using reflected light microscope.

Polished thin sections were examined under reflected light to characterize opaque minerals, including pyrite and associated iron oxides, which are opaque under transmitted light. Pyrite appears as bright, metallic, brassy-yellow crystals, often surrounded by reddish-brown oxidation halos, while iron oxides mark secondary alteration. Figures 4.8E and 4.9A–D illustrate these features, confirming sulphide mineralization and hydrothermal fluid interaction along structurally controlled pathways. Complementary observations of quartzite and schist reveal brittle deformation in quartzite promoting fluid ingress, and ductile shearing with recrystallization and intense alteration in schist near vein contacts. The presence of pyrite, iron oxides, and secondary micas supports a hydrothermal origin for gold deposits in the Nyakishenyi shear zone, emphasizing structural control by shear zones and faults.

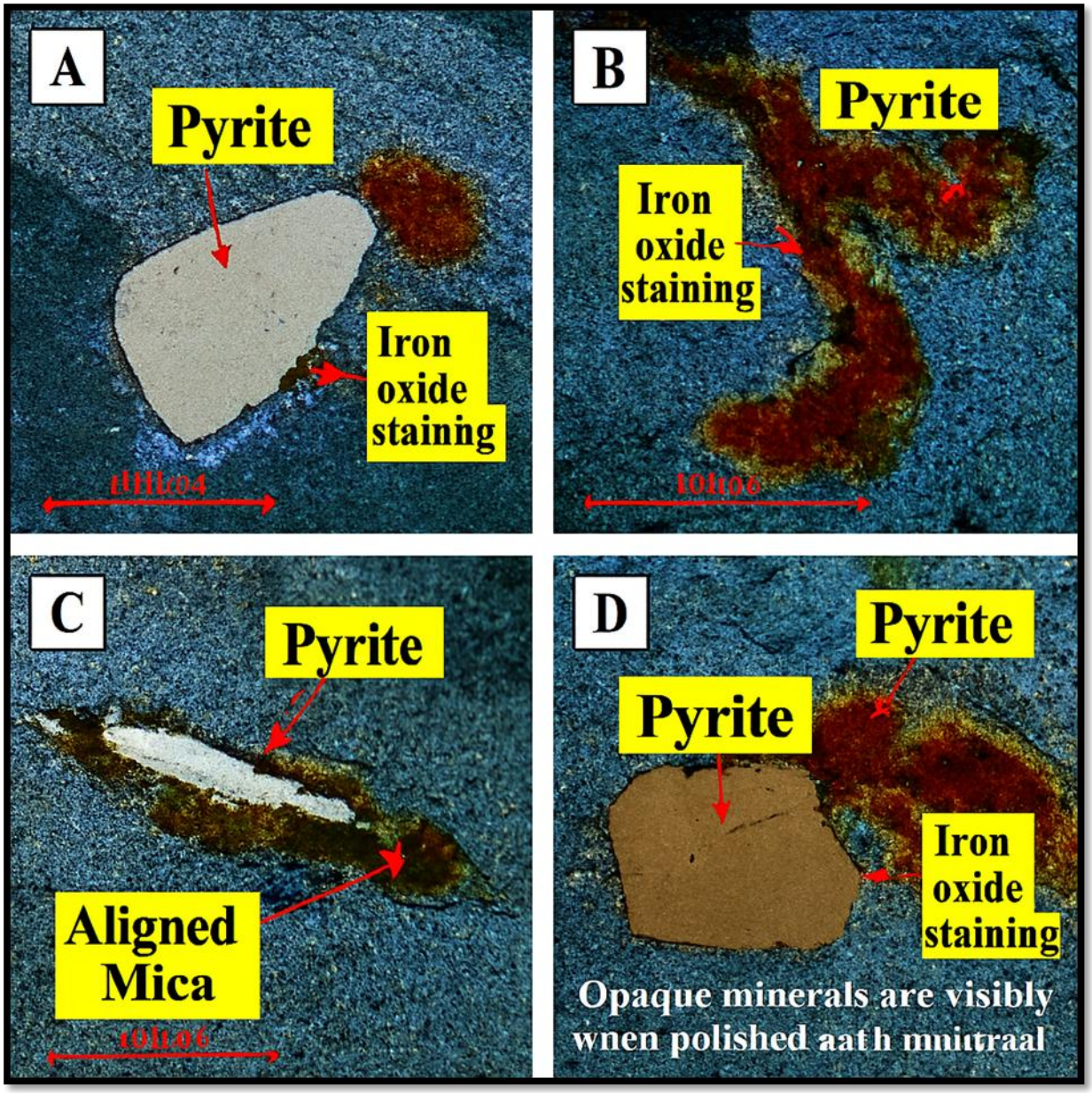

Figure 4.9A–D*: shows pyrite grains with metallic brassy-yellow luster and surrounding reddish-brown iron oxide halos. These textures indicate oxidative alteration and hydrothermal fluid interaction. The observations confirm structurally controlled sulphide mineralization in Nyakishenyi.*

These figures collectively demonstrate deformation-driven vein emplacement and hydrothermal cementation, reinforcing the orogenic gold model.

4.2.5 Wall rock and mineral assemblages.

i) Quartz alteration and muscovitization

Quartz in the Nyakishenyi shear zone exhibits hydrothermal alteration, including muscovitization and sericitization. Sulfide minerals are spatially associated with these alterations. Muscovitization involves the replacement of primary minerals such as biotite, plagioclase, and perthite by secondary muscovite or sericite.

Three main subtypes were identified:

a) Biotite → Muscovite: Biotite pseudomorphed by muscovite, often associated with iron oxides (Fig. 4.10A).
b) Plagioclase → Muscovite/Sericite: Fine-grained muscovite fibers within plagioclase laths (Fig. 4.10B).
c) Fracture and Vug Infilling: Muscovite fills granite fractures and dissolution vugs (Fig. 4.10B).

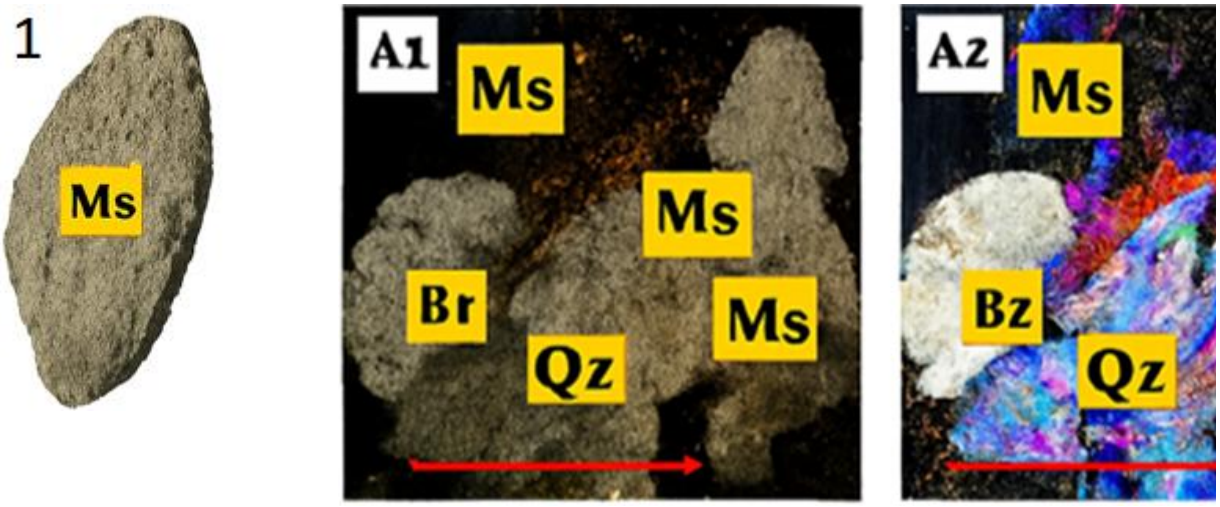

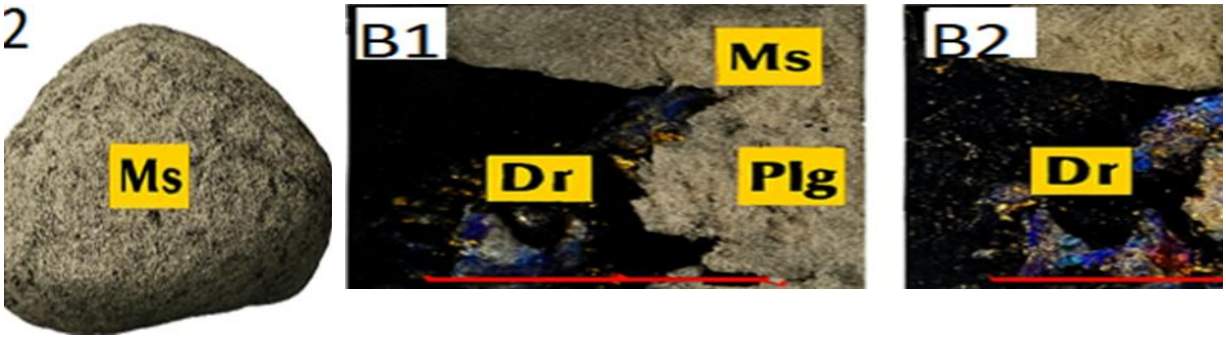

Figure 4.10. *A–B shows muscovite replacing biotite and infilling dissolution vugs. PPL highlights pleochroism, cleavage, and platy muscovite flakes, while XPL reveals interference colors and plagioclase twinning. These textures confirm hydrothermal alteration and secondary mineral growth associated with structurally controlled gold mineralization.*

ii) Granite alteration

Host granite around auriferous quartz veins exhibits a quartz–sericite–albite assemblage, typical of phyllic to argillic alteration. Coarse albite relicts are preserved within a fine-grained quartz–sericite–clay matrix (Figure 4.11), with sericite replacing feldspars and quartz remaining undeformed. Hand specimens show bleached zones and weathering halos, indicating pervasive fluid–rock interaction.

Under PPL, albite appears pale and fractured with sericite and clay infiltrating margins; XPL shows disrupted twinning and low birefringence in clay-rich zones, reflecting progressive plagioclase → sericite + clay + quartz replacement. Clay minerals (likely kaolinite or illite) are feldspar decomposition products, while quartz is a stable residual phase, confirming hydrothermal fluid-mediated alteration.

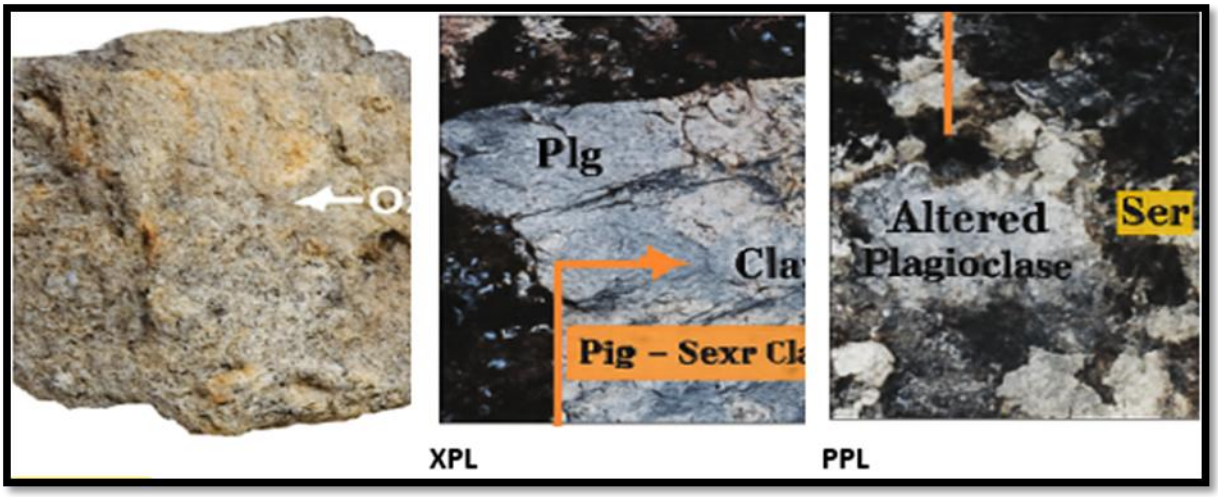

***Figure 4.11**: Quartz–sericite–albite assemblage showing albite relicts (Ab) partially replaced by sericite (Ser) and clay minerals (Cly), with quartz (Qz) as fine, undeformed grains. PPL highlights replacement textures; XPL shows disrupted twinning and low birefringence in altered zones.*

4.2.5 Mineralogy of ore

Polished sections from Nyakishenyi were examined under reflected light microscopy to characterize ore minerals, which include native gold, sulfides, and oxides within quartz veins and host granite.

4.2.5.1 Sulfide minerals

Sulfides make up ~5% of quartz veins. Pyrite is the most abundant, occurring in two generations:

Pyrite-I: Hypidiomorphic, found in least-altered granite, often containing rutile, wall rock, and minor pyrrhotite inclusions (Figure 4.12).

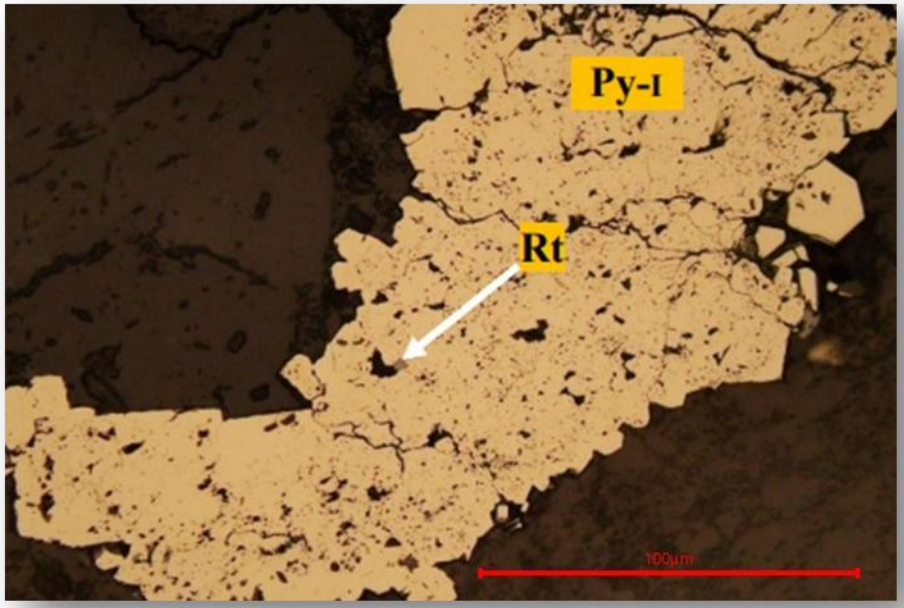

***Figure 4.12**: Xenomorphic pyrite-I (Py-I) in a quartz vein shows corroded contacts, with rutile (Rt) and wall rock inclusions visible under ambient light.*

Pyrite-II: Coarse-grained, disseminated in quartz veins, associated with arsenopyrite and fracture-fill minerals (Figures 4.13 & 4.14).

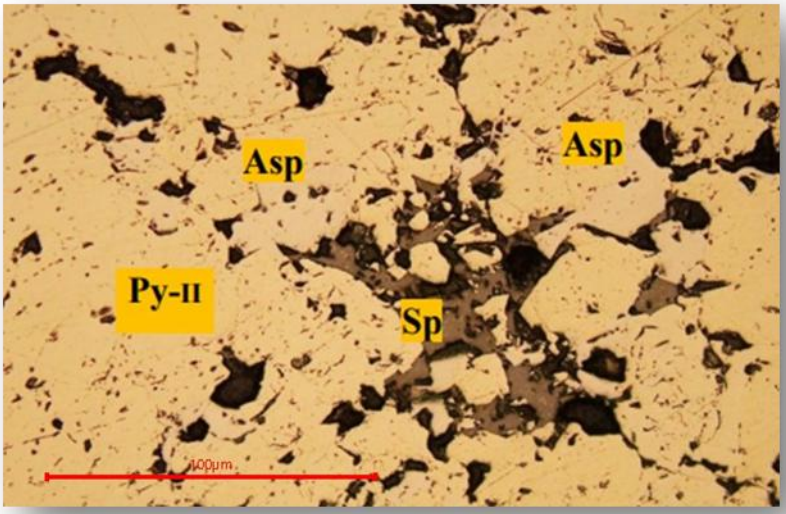

***Figure 4.13**: Coarse-grained pyrite-II (Py-II) associated with fracture-filling sphalerite (Sp) and idiomorphic arsenopyrite (Asp) under ambient light.*

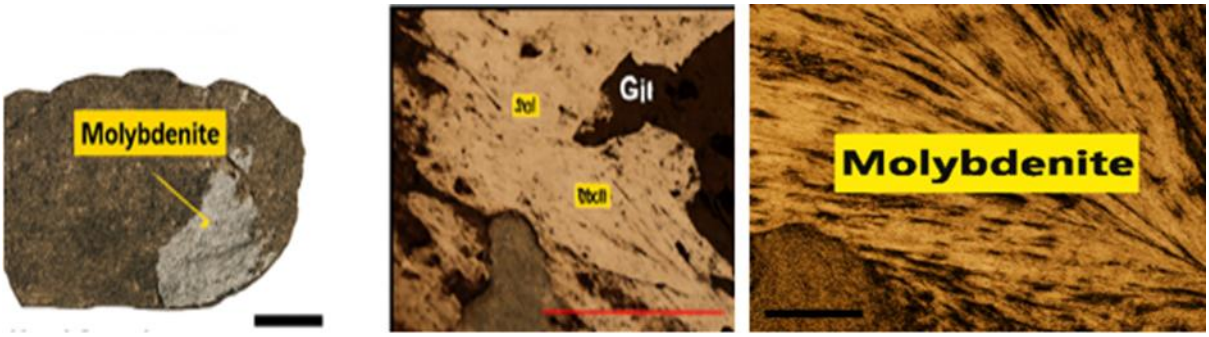

***Figure 4.14:** Gold (Au), galena (Gn), and chalcopyrite (Ccp) are inclusions in fracture-filling sphalerite (Sp) that are housed in deformed pyrite-II (Py-II). dry submersion in ambient light.*

Other sulfides include arsenopyrite (idiomorphic bipyramids, associated with pyrite-II and gold beads), sphalerite (isotropic, fracture-fill), chalcopyrite (minor, included in sphalerite), galena (microfracture-fill, intergrown with pyrite-II and molybdenite), molybdenite (platy, ductile, deformed along foliation), and trace pyrrhotite (<10 µm).

4.2.6 Paragenetic sequence

Mineralization in Nyakishenyi occurs in three main stages (Figure 4.15):

i) Pre-hydrothermal: Magmatic oxides (chromite, magnetite, pyrrhotite) in unaltered granite.

ii) Hydrothermal:

- Replacement textures: Pyrite-I, pyrite-II, arsenopyrite replacing pre-existing minerals.
- Fracture-fill textures: Pyrite-II, sphalerite, galena, chalcopyrite, native gold, and tellurides; accompanied by sericite, chlorite, calcite, and quartz.

iii) Supergene: Formation of covellite, goethite/lepidocrocite, and leucoxene during late-stage weathering.

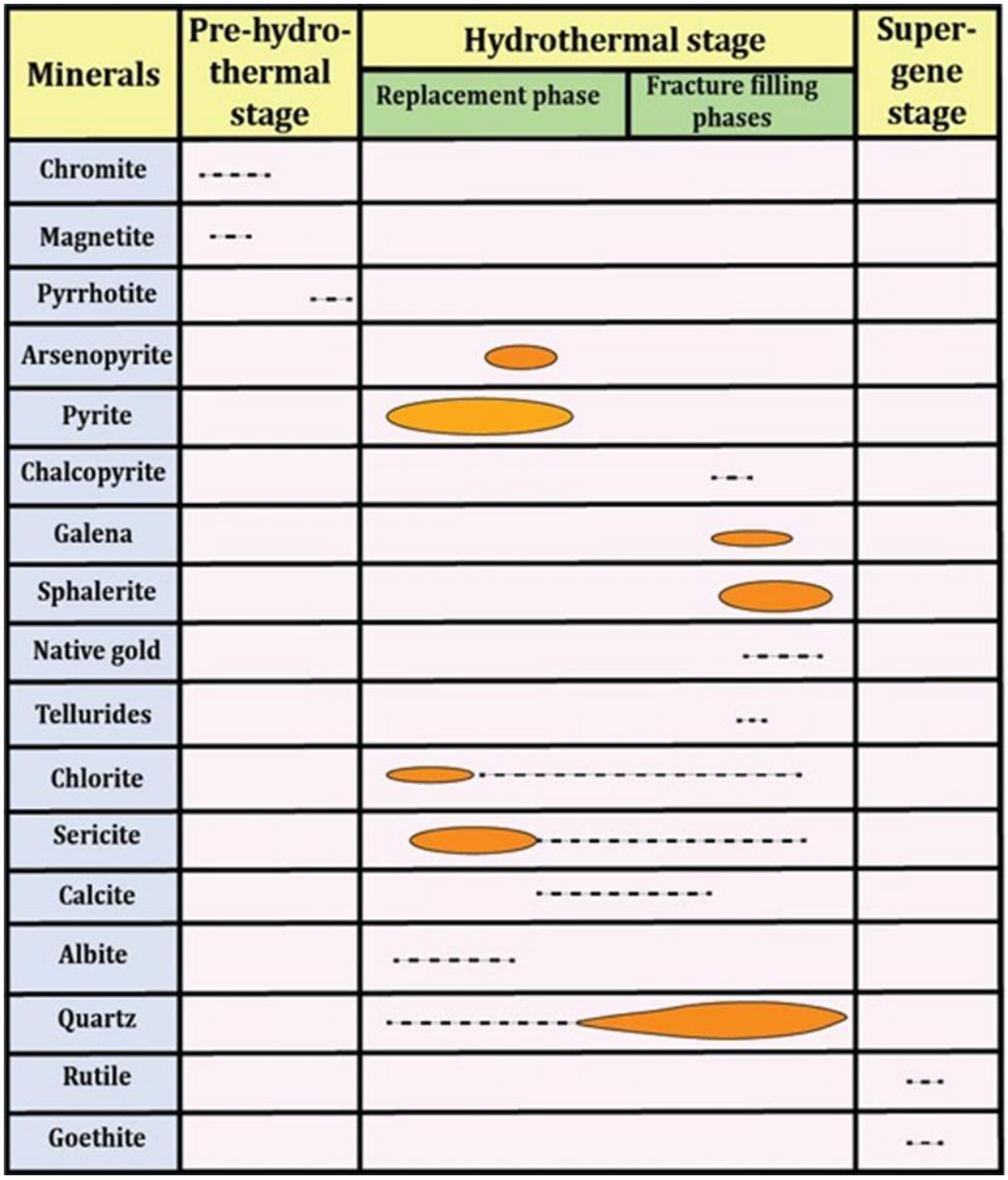

Figure 4.15: *illustrates multi-phase mineralization: early pyrite-I and rutile, hydrothermal replacement and fracture-fill sulfides, and late supergene oxides, confirming a structurally controlled hydrothermal system.*

4.3 Spatial distribution of gold deposits

Gold mineralization in Nyakishenyi is structurally controlled, with quartz veins, fault zones, and alteration halos concentrated in the central and northeastern parts of the study area, coinciding with artisanal workings (Figure 4.16). Integrated GIS mapping and systematic field traverses reveal that structural architecture strongly influences gold emplacement.

4.3.1 Geological and structural framework

The area is dominated by schists and quartzitic sandstones, mapped and georeferenced using ArcMap and GPS data (Figure 4.16). Schists are foliated, mica-rich, and exposed in valleys and low-lying areas, often displaying chlorite alteration (Figure 4.17). Quartzite interbeds and sandstones are massive, resistant, and mechanically competent, forming ridges and elevated outcrops. Their brittle nature favors fracture propagation, quartz vein emplacement, and gold-bearing systems.

Structural mapping recorded bedding, joints, and faults (Table 4.7). Quartz veins and shear zones align with these features, particularly along lithological contacts, indicating that vein emplacement is non-random and structurally controlled. Brecciated quartz veins and ferruginated quartz–sericite halos suggest multiple pulses of hydrothermal fluids, sulfide breakdown, and gold remobilization (Figure 4.18).

Table 4.7*: Summary of structural measurements in the Nyakishenyi area.*

Sample	**Easting**	**Northing**	**Feature type**	**Strike (°)**	**Dip (°)**	**Dip Direction**	**Lithological Context**	**Remarks**
NYK 01	205451.339	9972908.369	Bedding (Quartzite)	045–060	35–50	SE	Quartzite ridges	Consistent dip; minor folding near faults
Nyk 02	205689.7202	9971889.006	Bedding (Schist)	030–050	40–55	NW	Foliated schist zones	Locally overturned beds; tight

								folds
Nyk 03	206223.7889	9973019.385	Joint Set A	070–090	85–90	Vertical	Quartzite exposures	Open joints; some quartz infill
Nyk 04	205822.8635	9971853.310	Joint Set B	150–165	60–75	Sw	Schistose zones	Often mineralized with sulfides
Nyk05	206138.6157	9973200.555	Joint Set C	110–125	70–80	SE	Quartz veins & altered granite	Associated with molybdenite and galena
Nyk 06	205728.5329	9973225.945	Joint Set E	175–185	80–90	Vertical	Cross-cutting quartz veins	Late-stage brittle fractures; gold-bearing
Nyk o7	205748.8425	9972653.140	Fault Zone 1	050	70	SE	Quartz vein–wall rock contact	Major mineralized fault; cataclastic textures
Nyk 09	205910.9826	9972275.463	Fault Zone 2	120–135	45–60	SW	Altered schist margins	Shear zone with chlorite-sericite alteration

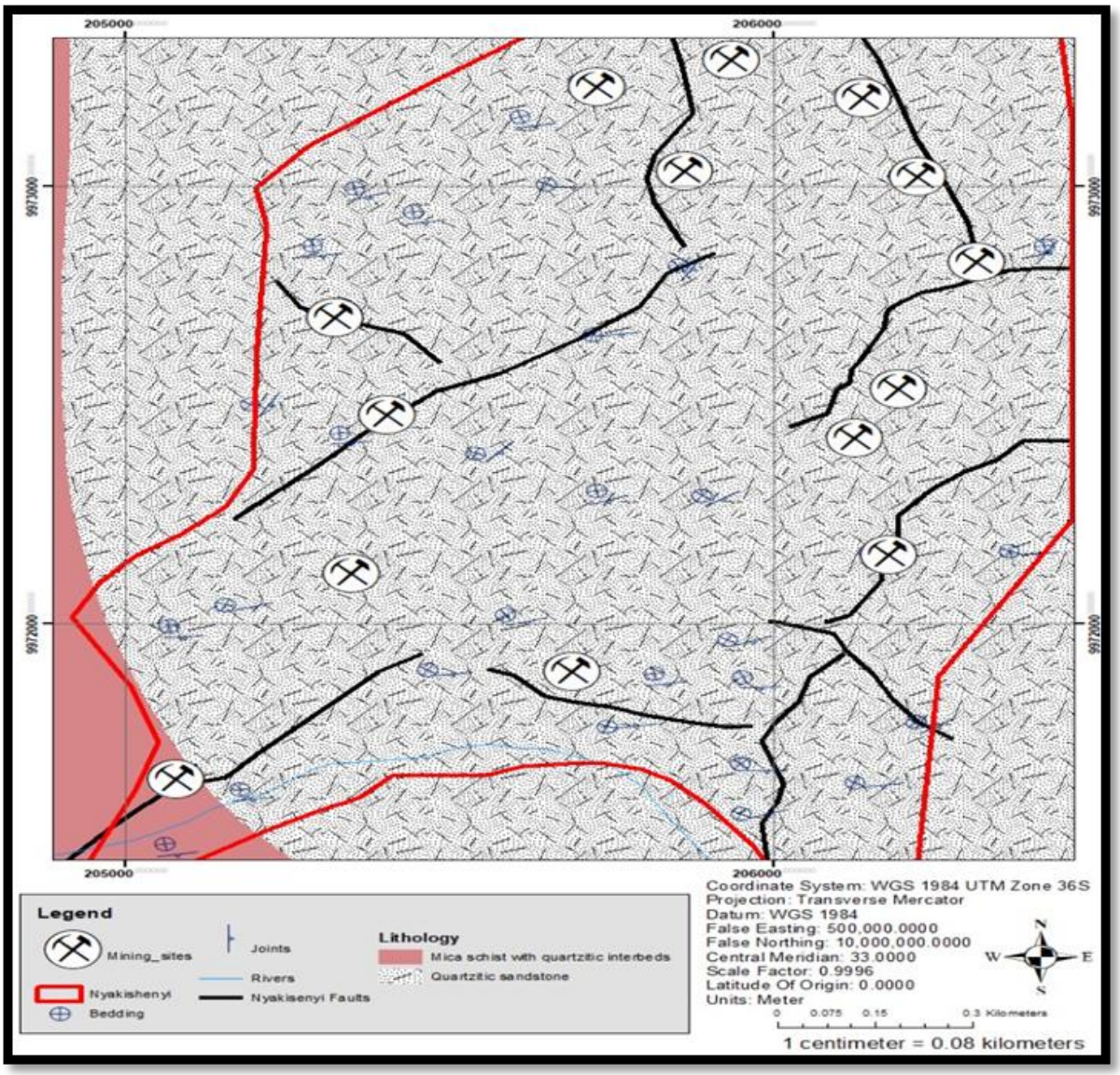

Figure 4.16: *Map showing different lithologies mapped in Nyakishenyi village with quartizitic sandstones being dominant lithology.*

Figure 4.17*. Picture showing mapped schists (grey to brown in color) associated with several platy foliations in the study area*

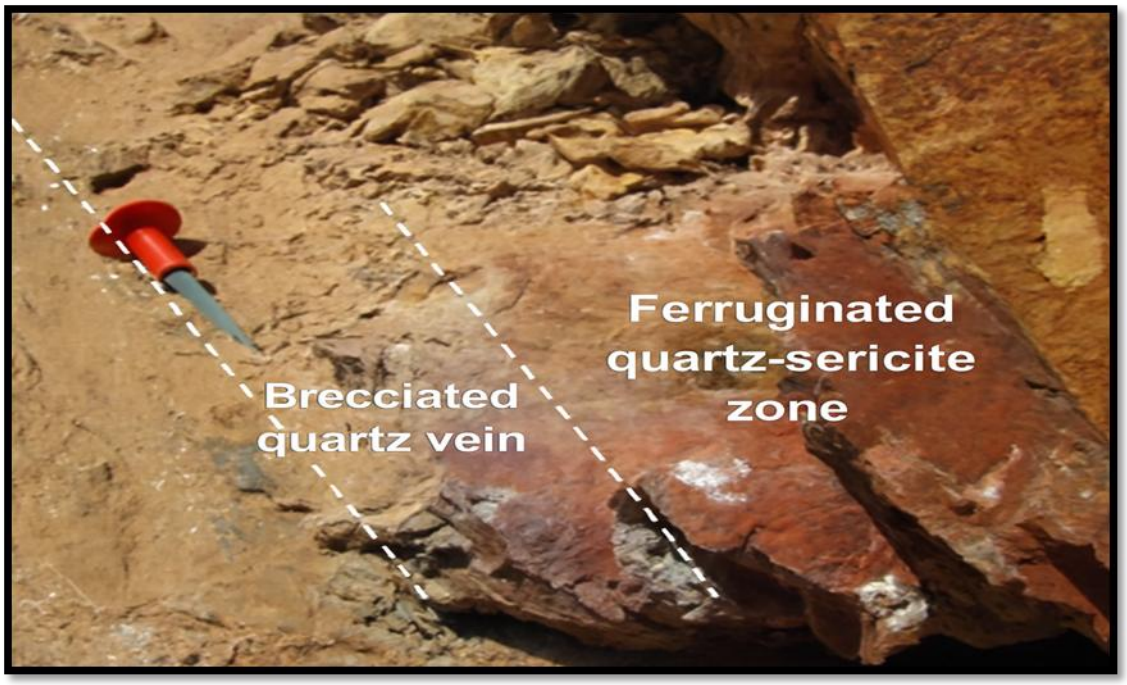

Figure 4.18*: Quartz outcrop demonstrates the structural and alteration controls on gold deposits in the study area by displaying a brecciated quartz vein in contact with a ferruginated quartz-sericite zone.*

4.3.2 Observations from artisanal mining pits

Artisanal pits provided key subsurface insights into lithology, structural orientation, and alteration textures (Figure 4.19). Most pits follow the NW–SE structural trend, consistent with shear zones and quartz vein orientations. Veins dip 45–70° towards the northeast and are associated with ferruginization, silicification, minor sulfides, and brecciated quartz fragments. Pit walls expose oxidized veins and intensely altered host rocks, confirming the structurally controlled emplacement of gold.

The combination of lithological contrasts, competent quartzites, reactive schists, and structurally localized quartz veins highlights the importance of structural and lithological controls on gold mineralization in Nyakishenyi. These findings provide a robust geological baseline for exploration and tectonic interpretation.

Figure 4.19*: Picture showing the mining pits at the site with exposures of different lithology at different soil horizons and the structures within the study area.*

4.3.3 Structural mapping and deformation features

Structural mapping in Nyakishenyi documented faults, folds, shear zones, joints, and foliation planes, highlighting their control on gold emplacement within the Buhweju–Mashonga gold district.

i) Major Fault Zones:

Several NW–SE and NE–SW trending fault zones were identified, cutting both schist and quartzite units (Figures 4.20 A-C)). Faults display slickensides, striations, brecciation, gouge zones, iron staining, and ferruginization, indicating brittle reactivation and hydrothermal fluid movement. Fault planes dip steeply (45–80°) and often host mineralized quartz veins along lithological contacts, acting as primary conduits for hydrothermal fluids and gold deposition.

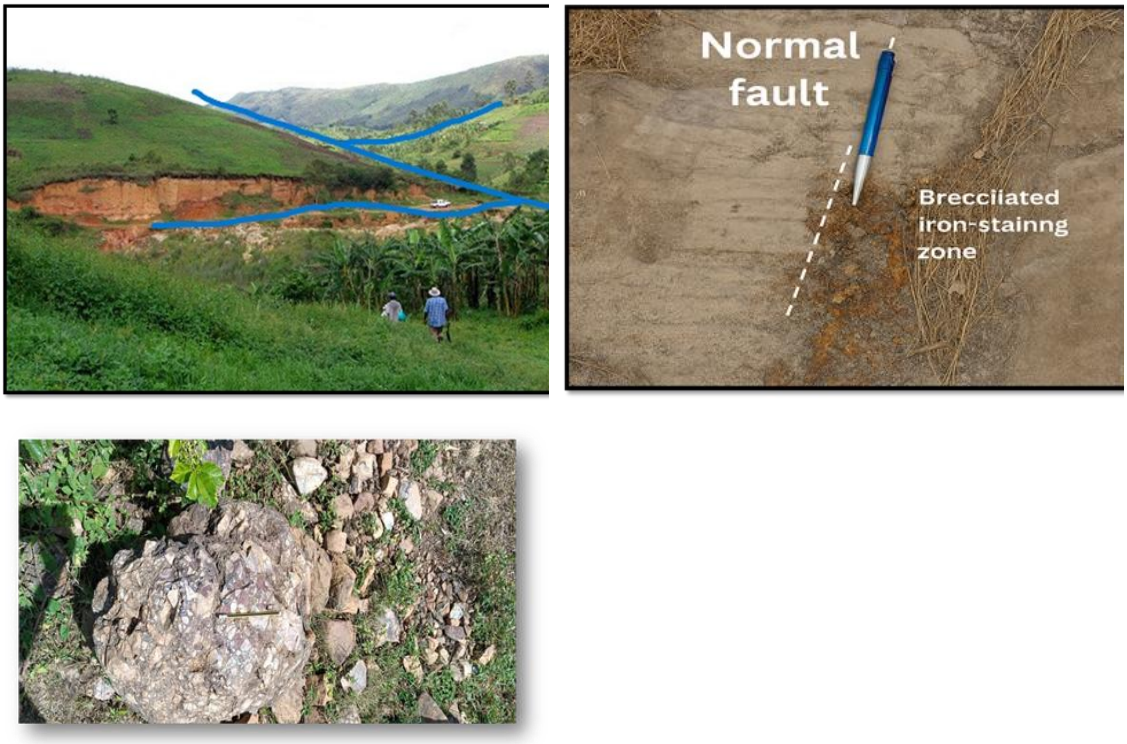

Figure 4.20A-C*: Showing the mapped geological features in Nyakishenyi;* ***A****-Fault plane,* ***B****-brecciated rock ,* ***C****-fault cutting in an outcrop.*

ii) Shear Zones:

NW–SE and N–S oriented shear zones are planar to sub-planar, meter-scale structures with ductile deformation, well-developed S–C fabrics, and asymmetric porphyroblasts. These features indicate both dextral and sinistral shear, suggesting multiple deformation phases and kinematic complexity.

iii) Joints:

Steeply dipping joints, generally orthogonal to foliation planes (Figure 4.21), enhance rock permeability and facilitated localized hydrothermal fluid flow, influencing gold concentration along structurally favorable zones.

Figure 4.21*: Jointed quartz–mica outcrop showing sub-parallel, steeply dipping joints aligned with regional structural trends.*

iv) Foliation Planes:

Schist units exhibit consistent foliation dipping moderately to steeply SW, defined by aligned mica flakes and quartz bands (Figure 4.22). Locally folded foliation reflects ductile deformation and frequently intersects quartz veins, indicating a structural control on vein emplacement.

Figure 4.22*: Field photograph showing well-developed foliation planes within metamorphosed quartzitic schist exposed on a hillside.*

v) Folding:

Minor to open folds in schist and quartzite units (tight to isoclinal in some areas) influence vein orientation and create spaces for fluid accumulation (Figures 4.17, 4.30). Fold axes generally trend NW–SE with cross-folding observed, increasing fracture density and permeability for hydrothermal fluids.

vi) Stereonet and fault density analysis:

Stereonet projections (Figures 4.23–4.28) show steeply dipping planes with predominant NE–SW strikes, aligning with field observations of quartz veins, joints, and fold limbs. Fault density maps (Figure 4.29) indicate structurally active corridors 30).along NW–SE and NE–SW trends, acting as pathways for fluid migration and gold mineralization.

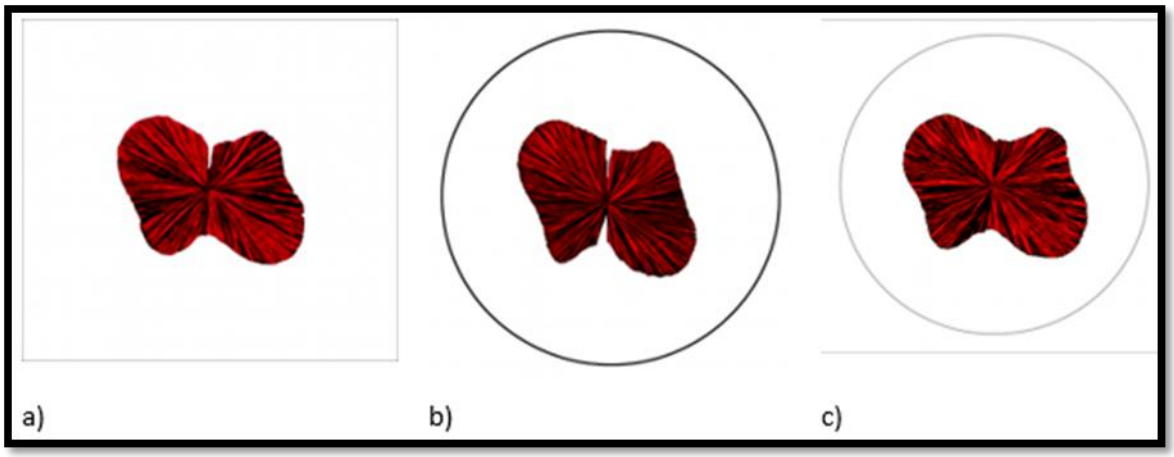

Figure 4.23a-c: Stereonet projection demonstrating the orientation of quartz veins, joints, and folds.

Structural features including faults, shear zones, joints, foliation, and folds control the localization of gold-bearing quartz veins. Multi-phase deformation, brittle reactivation, and hydrothermal alteration collectively enhanced permeability and created structurally favorable sites for gold deposition

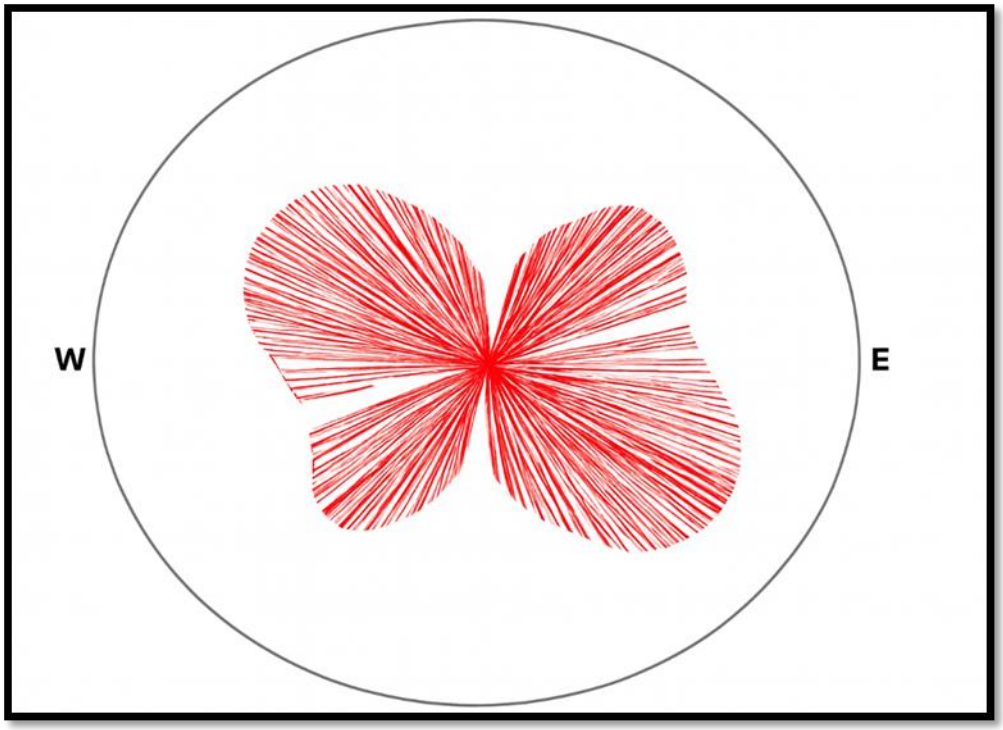

***Figure 4.24**: Stereonet illustrating the azimuthal distribution and frequency of structural features in the Nyakishenyi area.*

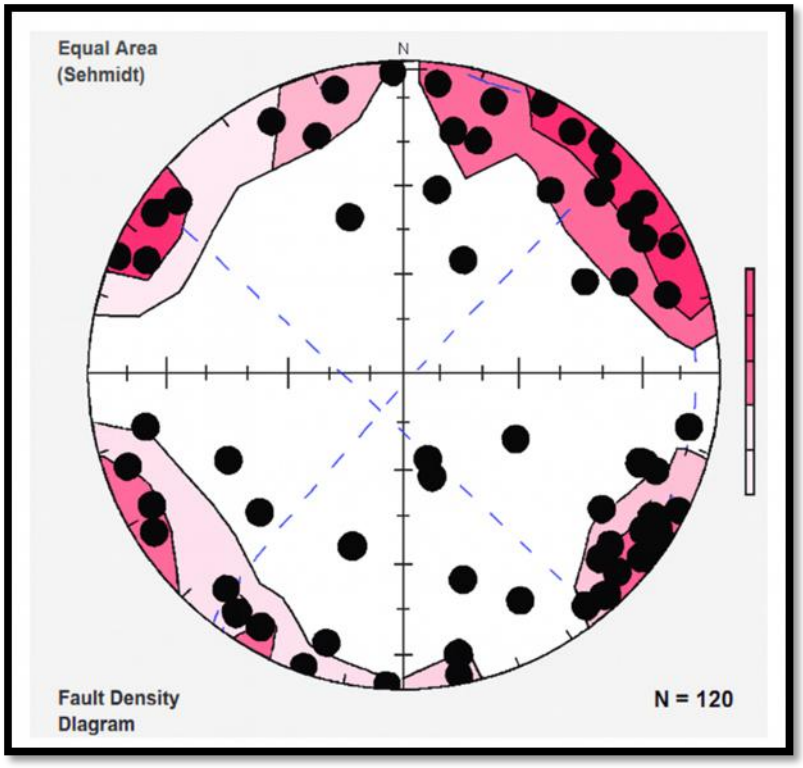

Figure 4.25: *Fault density diagram illustrating the spatial concentration and orientation of major and minor faults in the Nyakishenyi area.*

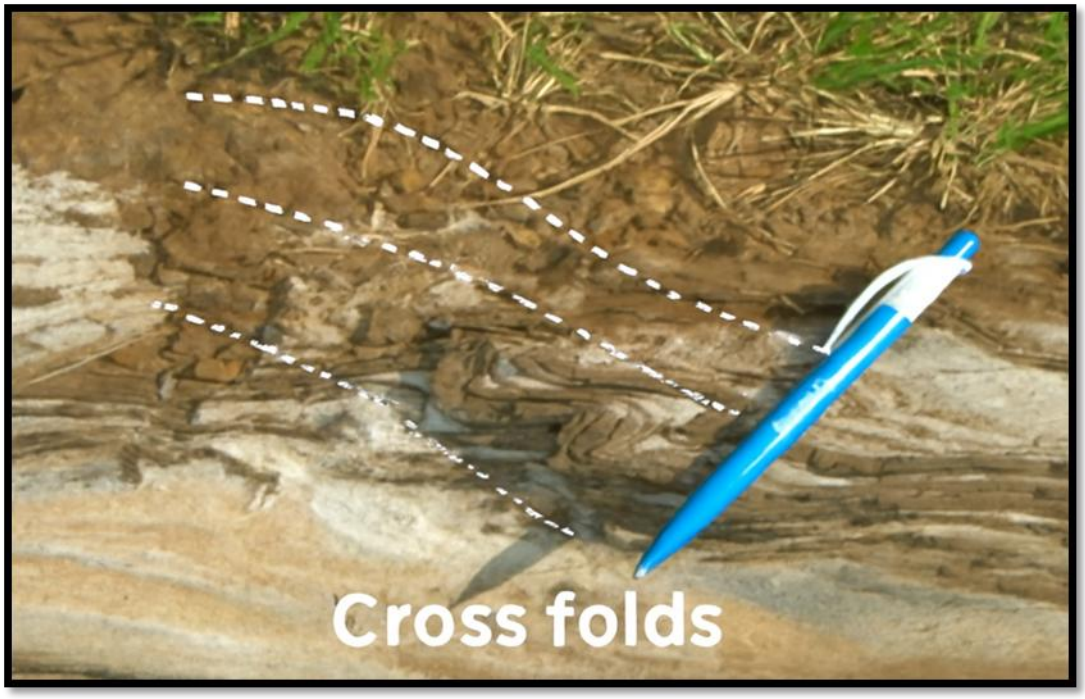

Figure 4.26: *Field photograph showing folded quartz outcrop with open folds.s*

Structural analysis shows a dominant NW–SE to NE–SW structural grain with steeply dipping planes. Stereonet and fault density data (Figures 4.24–4.25) indicate that quartz veins, joints, faults, and fold limbs share consistent orientations, forming structurally active corridors that focused hydrothermal fluid flow. Folded quartz outcrops (Figure 4.26) record compressional deformation and cross-folding, which increased fracture density and permeability. Together, these structures provided effective pathways for fluid migration and exerted strong control on quartz vein emplacement and gold mineralization at Nyakishenyi.

CHAPTER FIVE

DISCUSSION OF THE RESULTS

5.1. Determination of geochemical composition in primary and secondary gold ore occurrences

Geochemical data from rocks, soils, and stream sediments in Nyakishenyi reflect the combined influence of hydrothermal fluid activity, structural control, and supergene modification, rather than simple lithological variation (Tack et al., 2010; Backman et al., 2014). High SiO_2 values (70–79 wt.%) indicate quartz-rich host rocks and extensive veining, while elevated Al_2O_3 and Fe_2O_3 record intense hydrothermal alteration and weathering associated with sericitization and ferruginization along deformation zones (Backman et al., 2014).

Primary gold mineralization hosted in quartz veins shows sharp, high-amplitude elemental enrichments typical of focused hydrothermal deposition, whereas secondary soils and stream sediments display broader, diluted anomalies produced by mechanical dispersion and weathering. This contrast highlights the importance of integrating primary and secondary geochemical datasets when interpreting gold mineralization in structurally controlled systems (Goldfarb et al., 2001).

5.1.1 Enrichment of trace and pathfinder elements

Trace elements show strong enrichment of As, Sb, and W, confirming a sulfide-dominated hydrothermal gold system. Arsenic has the strongest correlation with gold ($r = 0.82$), indicating that gold precipitation was controlled by sulphidation and arsenopyrite stability under reduced, near-neutral to slightly acidic conditions typical of orogenic systems (Groves et al., 2020).

Weaker Au–Cu and Au–Zn correlations suggest decoupled or multi-stage mineralization, with base metals introduced during later or localized fluid pulses. Moderate Sb enrichment reflects late-stage or distal hydrothermal activity (Hale, 1981), while W enrichment and scheelite occurrence indicate high-temperature, deep-crustal fluid input. Mineralogical

associations of arsenopyrite, pyrite-II, stibnite, and scheelite confirm chemically evolving hydrothermal fluids during successive mineralizing events (Mäkitie et al., 2014).

5.1.2 Comparison of primary and secondary geochemical signatures

Primary gold occurrences in quartz veins show high concentrations of As, Sb, Cu, and W, reflecting direct hydrothermal deposition along structurally controlled zones (Groves et al., 2020). Secondary media, including stream sediments, exhibit lower, dispersed anomalies that still mirror primary signatures, indicating mechanical transport and genetic continuity with lode sources (Pohl, 2011).

The presence of sulfides (pyrite, arsenopyrite, chalcopyrite, galena) and a polymetallic signature (Au–As–Sb–Cu–Pb–Zn) confirms a mesothermal hydrothermal system controlled by fluid–rock interaction and structural conduits (Kampunzu et al., 2009). These patterns reinforce the value of integrating geochemistry with structural mapping for targeting primary mineralization and tracing secondary dispersion (Backman et al., 2014).

5.2. Characterization of gold deposits in Nyakishenyi Village

Gold deposits in Nyakishenyi are structurally controlled orogenic systems, occurring as primary lode veins and secondary/placer concentrations. Integration of geological mapping, petrography, and geochemistry indicates hydrothermal fluids precipitated gold along deformation zones, with subsequent redistribution into surface environments.

Primary deposits are hosted in quartz veins within schists and quartzites (<1 m thick), structurally aligned with NW–SE and NE–SW shear zones. These veins exhibit hydrothermal alteration (sericitization, silicification, ferruginization) and contain sulfides such as pyrite, chalcopyrite, and galena, consistent with mesothermal orogenic systems (Robert et al., 1997; Nyakecho & Hagemann, 2014).

Secondary and transitional deposits occur in lateritic soils, river sediments, and colluvial zones, formed by erosion and gravity-driven concentration of gold from primary veins. Transitional deposits in downslope colluvium represent an intermediate stage between lode sources and placer accumulations (Frimmel, 2005; Sillitoe, 2020).

Gold in Buhweju is predominantly orogenic, structurally controlled along NE–SW and NW–SE shear zones, hosted in schists, quartzites, and granitoid contacts, with geochemical enrichment in As, Sb, and W reflecting fluid–rock interaction during metamorphic devolatilization (Goldfarb et al., 2005; Oliver et al., 2020). Placer occurrences are secondary, representing surface expressions of deeper orogenic systems, useful for guiding upstream exploration.

5.3. Spatial distribution of gold deposits

Gold deposits in Nyakishenyi are structurally and topographically controlled, occurring along shear zones, faults, folds, and lithological contacts. Mineralized zones align with NE–SW and NW–SE trends, reflecting emplacement along fold axes, cross-fold structures, and conjugate shear zones of the Kigezi–Ankole Belt (Goldfarb et al., 2007; Kampunzu et al., 2009; Robert et al., 1997). Structural intersections, lithological boundaries, and elevated terrain enhance permeability, focusing hydrothermal fluid flow and gold precipitation. Polyphase deformation and fold interference patterns create structural traps that guide both primary quartz-vein and secondary placer deposits (Groves et al., 1998; Oliver et al., 2020).

Geochemical anomalies (Au, As, Sb, Cu, Pb, W) coincide with structural lineaments, fault density zones, and topographic lows, reflecting dispersion along erosion pathways and hydrothermal fluid conduits (Frimmel, 2005; Oliver et al., 2020). Primary quartz-sulfide veins dominate ridges, while secondary placer deposits accumulate in valleys and stream channels. Residual dispersion halos in lateritic soils and colluvial zones retain trace element signatures, providing indicators of upstream mineralization.

GIS integration enhanced spatial analysis by combining field-mapped lithology, structures, and geochemical data. Fault density mapping, overlay analyses, and structural–geochemical correlation identified high-potential zones at shear–fault intersections and lithological contacts (Nuwagira et al., 2023; Luís, 2018). These zones correspond with artisanal mining sites, validating predictive targeting approaches. Quantitative GIS tools—buffering, density mapping, and hotspot analysis—prioritized targets based on fault intensity, structural complexity, geochemical enrichment, and field alteration indicators, consistent with global

orogenic gold systems in the Ashanti Belt, Yilgarn Craton, and Kibaran Belt (Goldfarb et al., 2007; Groves et al., 2003).

In summary, gold in Nyakishenyi is concentrated where structural complexity, lithological contrasts, and geochemical anomalies converge. GIS-based structural and geochemical integration provides a robust framework for delineating primary lode targets and secondary placer zones, guiding efficient exploration in the Buhweju gold district.

5.4. Limitations of the study

The study's integration of structural, geochemical, and GIS datasets provided valuable insights into gold distribution in Nyakishenyi, but several limitations should be noted. Geochemical sampling was uneven due to difficult terrain and artisanal mining, potentially underrepresenting some anomaly clusters. Structural mapping relied on surface observations and satellite imagery, which may not capture minor or subsurface deformation critical to fluid pathways. The absence of geophysical data limited validation of subsurface structures and lithological continuity. GIS analyses were constrained by base map resolution and spatial accuracy, which could affect the identification of structural–geochemical convergence zones. Despite these constraints, the study demonstrates the utility of integrated exploration techniques, though future work with higher-resolution sampling, geophysics, and drilling is needed to refine models and improve exploration targeting.

CHAPTER SIX
CONCLUSION AND RECOMMENDATION

6.1. Conclusion

This study applied an integrated approach—combining geological mapping, structural analysis, geochemical assays, and GIS-based spatial modeling—to assess the genesis, distribution, and exploration potential of gold deposits in Nyakishenyi, Buhweju District. Results confirm that orogenic gold dominates the area, hosted in structurally controlled quartz–vein systems within schists, quartzites, and granitoid contacts. Mineralization is concentrated at shear–fault intersections, dilational zones, and NW–SE and NE–SW trending structural corridors, highlighting the primary role of structural permeability in guiding hydrothermal fluid flow and gold deposition, consistent with global orogenic gold models.

Geochemical analysis revealed significant Au anomalies associated with pathfinder elements (As, Sb, Cu, W), indicating fluid–rock interaction, sulfide precipitation, and alteration halos. Secondary placer deposits in stream sediments and colluvial zones were confirmed as erosional derivatives of primary lode systems, reinforcing the genetic link between primary and secondary gold occurrences. GIS integration of structural and geochemical data delineated high-potential zones, with fault density, anomaly overlays, and structural intersections correlating strongly with gold concentrations and artisanal mining activity.

Beyond local mapping, this study advances the regional metallogenic understanding of the Buhweju segment of the Kibaran Belt by demonstrating the interplay between structural architecture, fluid pathways, and element dispersion in controlling gold distribution. Future research should target underexplored structural intersections, apply high-resolution geophysics to validate subsurface structures, and conduct drilling to quantify ore grades and confirm prospective zones. These efforts will refine exploration models and enhance predictive targeting of orogenic gold deposits in the region.

6.2. Recommendations

Based on the findings of this study, the following recommendations are proposed to guide gold exploration, improve mining practices, and promote sustainable resource management in Buhweju District:

1. Target structurally favorable zones: Prioritize shear–fault junctions, fold hinges, and lithological contacts where geochemical anomalies converge, as these are high-potential sites for primary lode gold deposits.
2. Leverage artisanal workings as exploration guides: Systematically map and sample artisanal mining sites to trace alluvial gold back to upstream lode sources, enhancing exploration efficiency.
3. Refine structural and mineralization models: Conduct geophysical and geochronological investigations to understand subsurface structures, fluid pathways, and the timing of mineralization. Recommended methods include:

- Magnetic surveys to map hidden structures
- Resistivity and Induced Polarization (IP) to locate sulfide-rich zones
- Radiometric dating to constrain the timing of deformation and hydrothermal events

4. Expand GIS-based predictive exploration: Integrate geophysical, geochemical, and remote sensing datasets to develop process-based, predictive models for gold mineralization across Buhweju and the wider Kibaran Belt.
5. Promote sustainable mining and community engagement: Incorporate environmental management and capacity-building programs to minimize ecological impact, support responsible artisanal mining, and deliver socio-economic benefits to local communities.

Connect Buhweju to other structurally similar zones in the Kibaran Belt through collaborative programs involving government, academia, and industry. This will enable systematic exploration, process-based understanding, and responsible development.

These recommendations move beyond simple surface correlations and encourage a process-oriented approach, combining structural, geochemical, and geophysical insights to enhance gold discovery and sustainable resource management.

.

REFERENCES

Aanyu, K. (2011). Implications of regional fault distribution and kinematics for the uplift of rift flanks around the Rwenzori mountains, Southwestern Uganda [PhD Thesis]. Mainz, Univ., Diss., 2011.

Abraham, M. J., Gift, R., Hennery, S., Asuman, G., Rita, A., Dexter, D., & Joseph, M. (2020). The Prospects of Uganda's Iron Ore Deposits in Developing the Iron and Steel Industry. Journal of Minerals and Materials Characterization and Engineering, 8(4), 316–329.

AMBROSE, A. (2019). COLLEGE OF NATURAL SCIENCES [PhD Thesis]. Makerere University Kampala.

Backman, B., Salminen, R., Korkiakoski, E., Savolainen, H., Eklund, M., Turyasingura, P., & Muhwezi, D. K. (2014). Geochemical surveys in Uganda. Geol Survey Finland Spec Pap, 56, 74–120.

Bahiru, E. A. (2011). Inter-relationship between lithology and structure and its control on gold mineralization in Buhweju area, SW of Uganda [Master's Thesis]. University of Twente.

Bahiru, E. A., & Woldai, T. (2016). Integrated geological mapping approach and gold mineralization in Buhweju area, Uganda. Ore Geology Reviews, 72, 777–793.

Barnes, J. W. & others. (1961). The mineral resources of Uganda. Government Printer, South Africa.

Bauer, F., Karl, M., Glasmacher, U., Nagudi, B., Schumann, A., & Mroszewski, L. (2012). The Rwenzori Mountains of western Uganda–Aspects on the evolution of their

remarkable morphology within the Albertine Rift. Journal of African Earth Sciences, 73, 44–56.

Billa, M., Cassard, D., Lips, A. L., Bouchot, V., Tourlière, B., Stein, G., & Guillou-Frottier, L. (2004). Predicting gold-rich epithermal and porphyry systems in the central Andes with a continental-scale metallogenic GIS. Ore Geology Reviews, 25(1–2), 39–67.

Blevin, P. L. (2005). Intrusion related gold deposits. Geoscience Australia Open Files, Available At.

Bustillo Revuelta, M. (2017). Mineral deposits: Types and geology. In Mineral Resources: From Exploration to Sustainability Assessment (pp. 49–119). Springer.

Chen, Y.-J., Pirajno, F., Qi, J.-P., Li, J., & Wang, H.-H. (2006). Ore geology, fluid geochemistry and genesis of the Shanggong gold deposit, eastern Qinling Orogen, China. Resource Geology, 56(2), 99–116.

Cline, J. S., & Hofstra, A. A. (2000). Ore-fluid evolution at the Getchell Carlin-type gold deposit, Nevada, USA. European Journal of Mineralogy, 12(1), 195–212.

Cratchley, C. R., & Evans, R. B. (1967). Geophysical surveys for mineral deposits in area C/D, Western Uganda. (No Title).

Cunningham, C. G. (1985). Models for Epithermal Gold Deposition. Geologic Characteristics of Sediment-and Volcanic-Hosted Disseminated Gold Deposits–Search for an Occurrence Model, 1646, 43.

Data, G., Olarka, P., & Nyakecho, C. (2009). Gold Prospects in Uganda: Metallic Mineral Fact Sheets. Department of Geological and Mines, Uganda.

Davies, M. P., & Veillette, M. F. (2007). POGO PROJECT ALASKA–TAILINGS AND WATER MANAGEMENT FOR A COLD REGIONS MINE. Proc. Mining and the Environment 2007, 27–29.

Frimmel, H. E. (2005). Archaean atmospheric evolution: Evidence from the Witwatersrand gold fields, South Africa. Earth-Science Reviews, 70(1–2), 1–46.

Gabert, G. (1990). Lithostratigraphic and tectonic setting of gold mineralization in the Archean cratons of Tanzania and Uganda, East Africa. Precambrian Research, 46(1–2), 59–69.

Githenya, L. K. (2020). Geology and economic mineralization of the neoproterozoic Mozambique belt rocks of the Mwitika-Makongo area, Kitui County, South Eastern Kenya [PhD Thesis].

Goldfarb, R., Groves, D., & Gardoll, S. (2001). Orogenic gold and geologic time: A global synthesis. Ore Geology Reviews, 18(1–2), 1–75.

Goldfarb, R. J., Baker, T., Dubé, B., Groves, D. I., Hart, C. J., & Gosselin, P. (2005). Distribution, character, and genesis of gold deposits in metamorphic terran.

Goldfarb, R. J., Marsh, E. E., Hart, C. J., Mair, J. L., Miller, M. L., & Johnson, C. (2007). Geology and origin of epigenetic lode gold deposits, Tintina Gold Province, Alaska and Yukon. Recent US Geological Survey Studies in the Tintina Gold Province, Alaska, United States, and Yukon, Canada—Results of a.

Groves, D. I., & Bierlein, F. P. (2007). Geodynamic settings of mineral deposit systems. Journal of the Geological Society, 164(1), 19–30.

Groves, D. I., Goldfarb, R. J., Gebre-Mariam, M., Hagemann, S., & Robert, F. (1998). Orogenic gold deposits: A proposed classification in the context of their crustal distribution and relationship to other gold deposit types. Ore Geology Reviews, 13(1–5), 7–27.

Groves, D. I., Goldfarb, R. J., Robert, F., & Hart, C. J. (2003). Gold deposits in metamorphic belts: Overview of current understanding, outstanding problems, future research, and exploration significance. Economic Geology, 98(1), 1–29.

Groves, D. I., Santosh, M., Deng, J., Wang, Q., Yang, L., & Zhang, L. (2020). A holistic model for the origin of orogenic gold deposits and its implications for exploration. Mineralium Deposita, 55(2), 275–292.

Grynberg, R., Singogo, F. K., Grynberg, R., & Singogo, F. K. (2021). Gold and the Genesis of Modern African Resource Nationalism: The Cases of Tanzania and Ghana. African Gold: Production, Trade and Economic Development, 359–408.

Hale, M. (1981). Pathfinder applications of arsenic, antimony and bismuth in geochemical exploration. In Developments in Economic Geology (Vol. 15, pp. 307–323). Elsevier.

Herbert, S., Woldai, T., Carranza, E. J. M., & van Ruitenbeek, F. J. (2014). Predictive mapping of prospectivity for orogenic gold in Uganda. Journal of African Earth Sciences, 99, 666–693.

House, M. A., Wernicke, B. P., & Farley, K. A. (1998). Dating topography of the Sierra Nevada, California, using apatite (U–Th)/He ages. Nature, 396(6706), 66–69.

Jochum, K., & Verma, S. (1996). Extreme enrichment of Sb, Tl and other trace elements in altered MORB. Chemical Geology, 130(3–4), 289–299.

Kampunzu, A., Cailteux, J., Kamona, A., Intiomale, M., & Melcher, F. (2009). Sediment-hosted Zn–Pb–Cu deposits in the central African copperbelt. Ore Geology Reviews, 35(3–4), 263–297.

Kuehn, S., Ogola, J., & Sango, P. (1990). Regional setting and nature of gold mineralization in Tanzania and southwest Kenya. Precambrian Research, 46(1–2), 71–82.

Loayza-Tam, C. E. (2002). Geologic study of Cerro Yanacocha gold-silver deposit, Yanacocha district, northern Peru. University of Nevada, Reno.

Luís, A. M. (2018). Development of regional exploration techniques for groundwater resources in semiarid areas through integration of remote sensing and geophysical survey.

Mäkitie, H., Data, G., Isabirye, E., Mänttäri, I., Huhma, H., Klausen, M. B., Pakkanen, L., & Virransalo, P. (2014). Petrology, geochronology and emplacement model of the giant 1.37 Ga arcuate Lake Victoria Dyke Swarm on the margin of a large igneous province in eastern Africa. Journal of African Earth Sciences, 97, 273–296.

Mäkitie, H., Härmä, P., Virransalo, P., de Kock, G., Lugaizi, I., & Tumwine, A. (2008). The granite batholith of Mubende, Uganda: Preliminary results on its petrography, geochemistry and construction rock potential. GTK Consortium Geological Surveys in Uganda, 2012, 251–272.

Mao, J., Li, X., White, N. C., Zhao, C., Zhang, Z., Wang, Y., & Hu, H. (2007). Types, characteristics, and geodynamic settings of Mesozoic epithermal gold deposits in eastern China. Resource Geology, 57(4), 435–454.

Master, S., Bekker, A., & Karhu, J. A. (2013). Paleoproterozoic high δ13Ccarb marbles from the Ruwenzori Mountains, Uganda: Implications for the age of the Buganda Group. Chemical Geology, 362, 157–164.

Mavhungu, M. E. (2018). Evaluation of Nebulas Gold Deposit in Giyani Greenstone Belt, Limpopo Province, South Africa [PhD Thesis].

Monteiro, N. B. R., da Silva, E. A., & Neto, J. M. M. (2019). Sustainable development goals in mining. Journal of Cleaner Production, 228, 509–520.

Nokleberg, W. J., Brew, D. A., Grybeck, D., Yeend, W., Bundtzen, T. K., Robinson, M. S., Smith, T. E., Berg, H. C., Andersen, G. L., Chipp, E. R., & others. (1994). Metallogeny and major mineral deposits of Alaska.

Nuwagira, U., Mubiru, D., Igga, Y., & Nasasira, P. (2023). Impact of Artisanal Gold Mining on Wetland Health in Buhweju District, Southwestern Uganda.

Nyakecho, C., & Hagemann, S. (2014). An overview of gold systems in Uganda. Australian Journal of Earth Sciences, 61(1), 59–88.

Oliver, N. H., Allibone, A., Nugus, M. J., Vargas, C., Jongens, R., Peattie, R., & Chamberlain, V. A. (2020). The supergiant, high-grade, Paleoproterozoic metasedimentary rock-and shear vein-hosted Obuasi (Ashanti) gold deposit, Ghana, West Africa.

Phillips, G. N., & Powell, R. (1993). Link between gold provinces. Economic Geology, 88(5), 1084–1098.

Pohl, W. (1994). Metallogeny of the northeastern Kibara belt, Central Africa—Recent perspectives. Ore Geology Reviews, 9(2), 105–130.

Pohl, W. L. (2011). Economic geology: Principles and practice. John Wiley & Sons.

PRISCILLAH, M. (2022). A report on the geologic mapping of area C, Igayaza, Isingiro District, Western Uganda. Makerere University.

Reece, A. W. (1961). Explanation of the geology of sheet 76 (Buhwezu). (No Title).

Ressel, M. W., Dendas, M., Lujan, R., Essman, J., Shumway, P., Pennell, W., & Garside, L. (2015). Shallow expressions of Carlin-type hydrothermal systems: An example from the Emigrant mine, Carlin trend, Nevada. New Concepts and Discoveries, 1, 409–433.

Robert, F., Poulsen, K., & Dubé, B. (1997). Gold deposits and their geological classification. Proceedings of Exploration, 97, 209–220.

Schatzel, S. J., & Stewart, B. W. (2012). A provenance study of mineral matter in coal from Appalachian Basin coal mining regions and implications regarding the respirable health of underground coal workers: A geochemical and Nd isotope investigation. International Journal of Coal Geology, 94, 123–136.

Schlüter, T. (2008). Geological atlas of Africa (Vol. 307). Springer.

Schumann, A., Muwanga, A., Lehto, T., Staudt, M., Schlüter, T., Kato, V., & Namboyera, A. (2015). Ugandan geosites. Geology Today, 31(2), 59–67.

Serwajja, E., & Mukwaya, P. I. (2021). Environmental, health and safety intricacies of artisanal mining in the gold-rich landscapes of Karamoja, north-eastern Uganda. Journal of Sustainable Mining, 20(2), 90–108.

Sherlock, W. K. (2016). Interpretation of mineralization styles, alteration, mineralogy, paragenesis, and geochemistry at Gold Quarry, Carlin trend, Nevada: Implications for Northern Nevada-rift related, Miocene, intermediatesulfidation, base-metal mineralization. University of Nevada, Reno.

Sillitoe, R. H. (2020). Gold deposit types: An overview.

Staudt, M., Kuosmanen, E., Babirye, P., & Kedi, V. (2014). Production of multigeohazard maps for the Uganda Geological Mapping Project. Geological Survey of Finland, Special Paper, 56, 361–372.

Tack, L., Wingate, M., De Waele, B., Meert, J., Belousova, E., Griffin, B., Tahon, A., & Fernandez-Alonso, M. (2010). The 1375 Ma "Kibaran event" in Central Africa: Prominent emplacement of bimodal magmatism under extensional regime. Precambrian Research, 180(1–2), 63–84.

Taylor, R. D. (2015). Orogenic gold formation and tectonic evolution of the Grass Valley gold district and temporal correlations of gold deposits in California. Colorado School of Mines.

Thomas, R. J., Spencer, C., Bushi, A. M., Baglow, N., Boniface, N., de Kock, G., Horstwood, M. S., Hollick, L., Jacobs, J., Kajara, S., & others. (2016). Geochronology of the central Tanzania Craton and its southern and eastern orogenic margins. Precambrian Research, 277, 47–67.

van der Ven, M. J. (2020). An overview of recent developments and the current state of the Ugandan energy sector. International Growth Centre.

Wayland, E. J. (1934). Rifts, rivers, rains and early man in Uganda. The Journal of the Royal Anthropological Institute of Great Britain and Ireland, 64, 333–352.

Woldai, T., & Fabbri, A. G. (2022). Data Mining of a Geoscience Database Containing Key Features of Gold Deposits and Occurrences in Southwestern Uganda: A Pilot Study. Natural Resources Research, 31(5), 2289–2319.

APPENDICES

Table A 1: *Sampling results*

Sample ID	Sample_Type	Easting	Northing	SiO2	TiO2	Al2O3	Fe2O3	MnO	MgO	CaO	Na2O	K2O	P2O5	Au	Ag	As	Ba	Ce	Co	Cr	Cu	Ga
S1	Soil	205870.7	9972447	69.64385	0.646507	15.62891	3.078385	0.067671	1.283879	1.343798	2.357569	2.848156	0.319408	2.522076	0.442616	29.84869	462.4068	37.36111	9.720419	88.33065	45.67557	16.07163
S2	Soil	205605.6	9971995	78.54406	0.569501	17.17727	2.851023	0.04441	1.621236	0.920025	2.159467	3.182145	0.213212	0.101497	0.616456	21.69877	417.8314	38.92374	13.52739	93.20613	51.29602	16.51385
S3	Rock	205451.3	9972908	79.37934	0.552473	14.677	3.115427	0.063824	1.489261	1.780418	2.598232	2.299343	0.253679	1.980902	0.568563	25.16113	452.6327	31.59854	12.51459	88.15377	50.56338	18.03508
S4	Sediment	205362.6	9972965	64.88078	0.722022	12.22121	3.22995	0.043925	0.868446	1.911188	2.688365	3.653823	0.167676	2.899052	0.614412	29.5138	443.5574	32.24945	14.2119	81.05391	48.18119	19.02019
S5	Sediment	206138.6	9973201	76.94926	0.567985	14.42317	3.145348	0.071737	0.565931	2.038897	2.080052	3.077714	0.266978	3.566051	0.581415	33.039	463.5307	34.45333	10.17537	86.86604	50.90908	16.34888
S6	Soil	205863.8	9973032	66.27503	0.917428	13.50299	2.178772	0.04066	1.685476	0.835602	1.631101	2.53359	0.228134	3.710002	0.371013	31.84014	471.3643	34.45764	14.21396	87.68829	51.62386	20.48078
S7	Rock	205077.2	9971644	68.71194	0.750912	14.87412	3.045675	0.075898	1.111072	1.489359	1.749867	3.403556	0.258673	4.509654	0.539187	26.98751	519.1892	31.70762	13.12815	74.73708	45.78862	20.90267
S8	Sediment	205935.3	9973288	72.85274	0.712195	13.68428	3.232079	0.063131	1.272525	1.436011	1.902438	3.133773	0.191894	3.418279	0.59983	30.30119	442.5437	40.35985	12.55747	90.67532	52.26077	22.95853
S9	Rock	206223.8	9973019	74.79807	0.577937	14.58599	2.896854	0.04572	1.319547	1.534184	2.0644	4.014193	0.155912	2.445398	0.561732	34.25811	461.2069	36.09196	13.66617	87.02715	38.63894	19.70007
S10	Rock	206126	9972423	63.6357	0.577024	16.69555	2.785738	0.059887	1.154116	1.101743	2.675626	3.256429	0.29276	2.819535	0.741496	27.01552	432.4335	39.42493	13.6632	84.3588	48.3092	17.84578
S11	Sediment	206194.4	9972535	71.23461	0.733663	14.42865	2.800376	0.065976	0.999381	1.917358	1.78678	2.893449	0.346548	0.54236	0.724041	21.58495	443.5163	37.61781	12.13138	86.77883	47.87486	18.96777
S12	Sediment	206177.8	9972157	71.15145	0.884043	15.53245	2.932664	0.056336	1.287486	1.858743	2.807636	2.848209	0.306408	0.591668	0.552669	25.31487	445.7916	34.92349	15.48568	91.99549	43.2379	16.38301
S13	Rock	205689.7	9971889	75.95883	0.536579	13.52312	2.784951	0.05905	1.109821	1.326794	1.657248	3.289512	0.199372	0.183178	0.796698	18.59485	465.3494	31.23506	11.11195	84.71788	45.81318	19.88944
S14	Sediment	205674.7	9972991	63.99838	0.619126	15.84341	2.974906	0.07304	0.893192	1.487035	2.37269	3.845363	0.346732	0.563276	0.811958	21.04789	470.2368	34.81629	14.16826	92.00045	46.55159	17.20565
S15	Sediment	205182.4	9972029	67.48698	0.559845	12.12575	3.136538	0.067095	1.029545	1.891043	2.093133	3.361106	0.269312	0.076792	0.54758	24.0949	432.6841	36.95826	10.70107	87.0461	51.00275	20.4513
S16	Rock	205569.2	9972380	72.75647	0.665762	14.71254	2.395644	0.074512	0.751822	1.27684	1.704314	3.70757	0.220829	2.333491	0.565691	28.47669	475.0175	41.42176	11.48346	92.71177	49.76757	22.51281
S17	Rock	205748.8	9972653	64.49527	0.509312	15.48096	2.979541	0.057214	1.380103	1.64886	1.546939	3.384085	0.290085	2.299376	0.564793	29.09775	513.099	37.23032	12.51986	81.5622	44.74296	17.95618
S18	Sediment	205980	9971552	60.97153	0.698446	14.42244	2.920785	0.048321	0.979978	1.06144	1.930039	3.720247	0.328031	3.141093	0.655916	28.50482	463.4055	43.832	14.00169	81.83475	45.4713	22.08648
S19	Sediment	205771.5	9971758	72.40975	0.686036	15.35191	2.32523	0.051803	1.186801	1.755137	2.346959	3.887847	0.19187	2.642877	0.627741	28.09597	479.668	37.50443	16.18558	85.29742	47.09858	17.03219
S20	Sediment	206392.7	9972153	70.94052	0.784983	14.99029	3.78336	0.056597	1.228912	1.600065	1.878235	3.338831	0.232037	0.0005	0.489087	17.64202	468.9387	37.06371	11.06496	89.48713	51.88177	17.00506
S21	Rock	206153.1	9971623	74.49045	0.790728	15.17351	3.309931	0.065116	0.686688	1.81597	2.641208	3.105546	0.272946	2.028917	0.439676	26.06345	481.0919	33.80147	14.59255	85.86175	41.4889	20.40463
S22	Rock	205822.9	9971853	71.13436	0.691503	15.31294	3.882864	0.063837	1.377768	1.684206	1.580749	2.654937	0.332652	3.644454	0.297764	30.87949	495.0238	36.22537	13.11814	84.31082	47.19106	18.69967
S23	Soil	205074.4	9971961	78.7747	0.673221	14.96656	2.434988	0.054955	1.157825	1.476247	1.637065	3.204897	0.315936	2.691382	0.585739	30.06402	443.8934	34.02879	13.03385	90.798	53.67646	16.31317
S24	Soil	205331.5	9972406	69.77565	0.672745	13.08977	3.288614	0.048995	0.884879	1.03029	2.847702	3.19777	0.256619	1.306297	0.835554	27.5729	452.8203	35.65659	12.79212	88.73658	52.08557	18.7915
S25	Rock	205973.9	9971660	62.72186	0.67538	18.17718	2.530283	0.059652	0.914413	1.39388	2.217881	3.488287	0.22778	2.465941	0.720511	32.23835	436.3276	36.71548	12.72726	93.46776	48.14154	17.42822

S26	Sediment	205068.2	9971464	3.304723	1.650253	34.21428	63.5021	124.8489	2.212069	9.171531	6.137417	310.6255	1.042394	4.822947	2.277617	116.757	0.837688	20.82809	101.027	173.2514
S27	Sediment	205220.1	9972487	3.257661	1.467647	34.70285	64.10649	102.6193	2.50121	9.384092	5.615167	322.342	0.795492	4.078295	2.392063	113.2573	0.681945	22.85654	98.27432	160.5351
S28	Soil	206121.7	9971343	2.948064	1.486568	31.93492	56.83524	146.5548	1.949218	8.964971	5.797704	299.4664	0.893445	4.597658	2.549206	109.2246	1.073833	21.00586	90.39944	175.4415
S29	Sediment	205349.3	9972114	3.824471	1.326157	37.52147	55.50457	123.0167	2.556752	10.88573	5.223428	295.7116	0.87705	4.095434	2.325389	118.0324	1.062568	23.91131	86.64421	168.2338
S30	Rock	205728.5	9973226	2.778297	1.461679	31.95135	66.52176	133.5894	2.154954	10.05759	5.74115	283.6545	0.925965	5.189332	2.150316	107.6534	0.967788	26.1959	102.4986	172.3021
S31	Rock	205323.6	9972698	3.319697	1.507628	35.34941	61.99809	119.4678	2.377609	8.656964	5.584529	309.679	1.036051	5.338311	2.432959	104.1228	0.916216	22.82633	92.45555	143.0001
S32	Rock	206314.4	9972826	3.482941	1.534839	34.1031	59.20762	130.8053	2.551981	7.065577	6.457346	279.586	0.757615	5.081487	2.198915	106.5126	0.804908	25.73526	100.4371	169.337
S33	Rock	205404.2	9972477	2.899493	1.508996	31.13894	58.63213	119.6811	2.303745	10.91756	6.422173	316.4659	0.943859	4.447711	2.531603	121.4138	0.865242	24.8478	99.80417	151.5691
S34	Soil	206175.1	9973592	4.303633	1.577078	33.18974	53.87997	127.6648	2.643369	10.82137	5.20235	313.7536	0.879551	4.996059	2.118687	109.8238	1.095121	23.59627	98.82882	164.4186
S35	Sediment	205618.9	9973127	3.921381	1.346814	29.36442	71.97689	132.613	2.297262	9.759718	5.10151	314.0336	0.786225	3.727359	2.654337	114.1454	0.807583	21.30405	94.74268	170.4829
S36	Sediment	205964.3	9971848	3.382042	1.493404	36.45259	64.87086	116.3386	2.376889	10.34231	5.180384	297.0251	0.900242	4.119339	2.668655	113.6895	0.873263	25.55756	97.9994	164.596
S37	Soil	206243.7	9971757	3.210615	1.658567	35.72368	65.4297	137.9001	2.44132	9.877803	5.029607	310.9794	0.991358	5.634299	2.554989	110.5868	0.925042	23.7639	99.7053	150.429
S38	Rock	205871.7	9972796	3.494242	1.487725	32.87939	64.45846	131.7355	2.338981	10.28689	6.300666	290.6989	1.027341	4.342546	2.806005	122.381	0.914247	25.71733	86.29727	165.6446
S39	Soil	206420.3	9972834	3.14607	1.536559	33.35579	63.69112	116.9142	2.512169	10.36817	5.575682	296.8742	1.018271	5.365732	2.28436	107.836	0.971623	22.88046	93.03161	166.9775
S40	Sediment	205756.5	9973441	2.743411	2.081531	31.57763	68.3625	111.4393	2.311714	9.709695	5.971411	290.3765	1.010951	4.396692	2.40771	116.4428	0.983358	24.54712	88.98216	177.577
S41	Rock	205292	9972832	3.504445	1.518409	31.48691	61.87294	116.6141	2.426854	11.90318	6.491693	277.7781	0.90364	4.20673	1.989804	111.2184	1.069625	20.93483	101.0221	167.9057
S42	Rock	205956.1	9971949	3.275262	1.508795	29.40379	59.84418	127.016	2.294155	9.855019	6.627798	295.7317	0.933507	3.778957	2.350308	112.9096	0.882528	21.16935	93.51618	171.9443
S43	Soil	205487.6	9971877	3.491753	1.544684	27.59404	52.74104	129.2011	2.269202	9.427736	6.568467	312.4102	0.837769	4.815218	2.236541	107.9323	0.987675	23.29388	97.59237	154.9371
S44	Rock	205911	9972275	3.403641	1.210526	30.13959	60.92744	128.1274	2.004915	9.500782	4.951054	284.1076	1.086776	4.978099	2.633362	111.5585	1.093456	23.74402	93.21253	184.7672
S45	Sediment	205734.6	9972272	3.33722	1.504471	31.46049	69.75503	140.2517	2.067841	11.25312	5.295411	318.2551	0.876551	3.998487	2.692141	117.1446	1.07999	22.08721	101.7875	162.618
S46	Soil	205179.3	9971591	3.292293	1.740408	31.46505	60.24313	116.5846	2.193236	9.545581	5.942081	308.8176	0.836643	5.006034	2.24186	104.119	0.910213	22.66924	95.26125	176.5303
S47	Soil	205154.6	9971738	3.777766	1.49021	31.96962	63.06345	96.24833	2.154632	10.10955	5.824929	288.6257	0.950954	4.362763	2.605699	111.063	1.018674	25.15522	97.25243	157.5379
S48	Sediment	206011	9973518	3.178566	1.552362	32.00226	68.88881	132.7816	2.584194	9.992641	5.944537	299.8599	0.841681	4.687687	2.371329	110.8323	1.010242	23.48669	95.81901	165.8814
S49	Rock	206405.2	9973056	3.111261	1.930274	29.29528	65.97887	121.2752	2.405944	9.418042	5.469221	329.0159	0.695096	3.91069	2.331484	104.7849	1.112554	20.76634	100.4356	163.8543
S50	Sediment	206375.7	9972325	3.283542	1.496312	33.64954	59.15745	134.1062	2.320177	9.996302	6.582683	306.176	0.989467	5.509421	2.400216	111.743	0.839499	22.27277	97.61282	159.2751

Table A 1.2: Results from mining sites

Sample Name	Sample type	Eastings	Northings	Au values
S5	sediment	206405	9973056	4.33572
S23	Soil	206139	997320	3.56605
S49	rock	205074	997196	2.69138

As (up to 6.3 ppm), Sb (0.3–0.7 ppm), and W (0.8–0.97 ppm), alongside Cu, Pb, and Zn